Magnetic anisotropy and slow magnetic relaxation processes of cobalt(II)-pseudohalide complexes

Hui-Hui Cui,[a] Yi-Quan Zhang,*[b] Xue-Tai Chen,*[a] Zhenxing Wang,*[c] and Zi-Ling Xue[d]

[a]*State Key Laboratory of Coordination Chemistry, School of Chemistry and Chemical Engineering, Nanjing University, Nanjing 210023, China*

[b]*Jiangsu Key Laboratory for NSLSCS, School of Physical Science and Technology, Nanjing Normal University, Nanjing 210023, China*

[c]*Wuhan National High Magnetic Field Center, Huazhong University of Science and Technology, Wuhan 430074, China*

[d]*Department of Chemistry, University of Tennessee, Knoxville, Tennessee 37996, USA.*

Electronic Supplementary Information

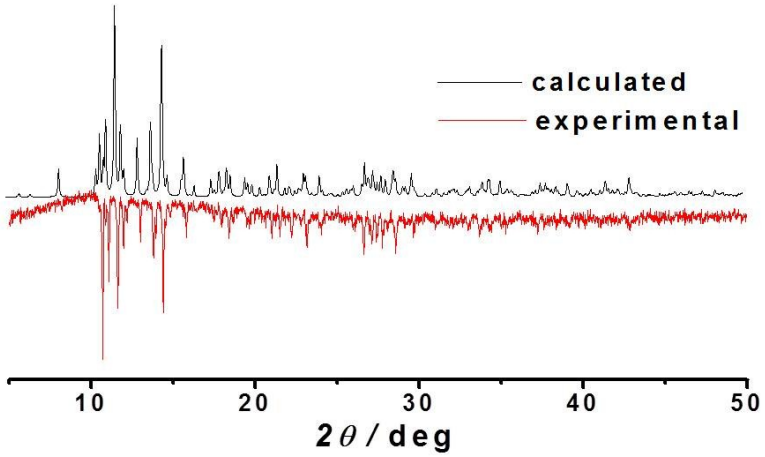

Fig. S1 XRD patterns for complex **1**.

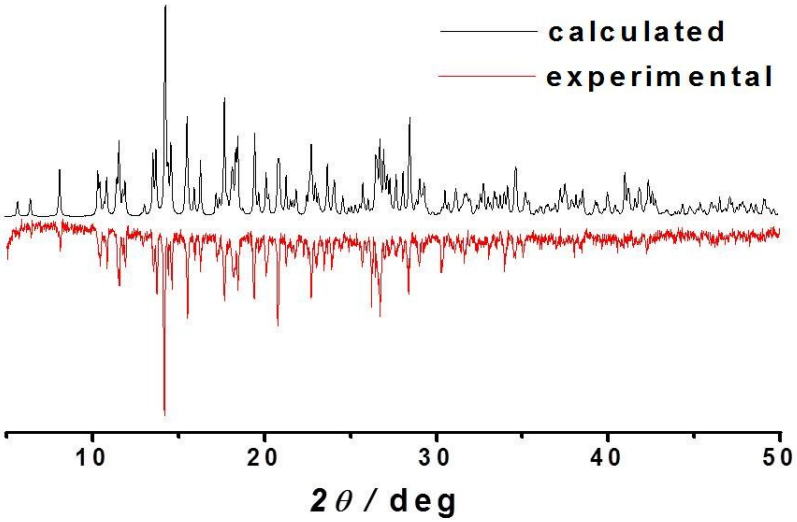

Fig. S2 XRD patterns for complex **2**.

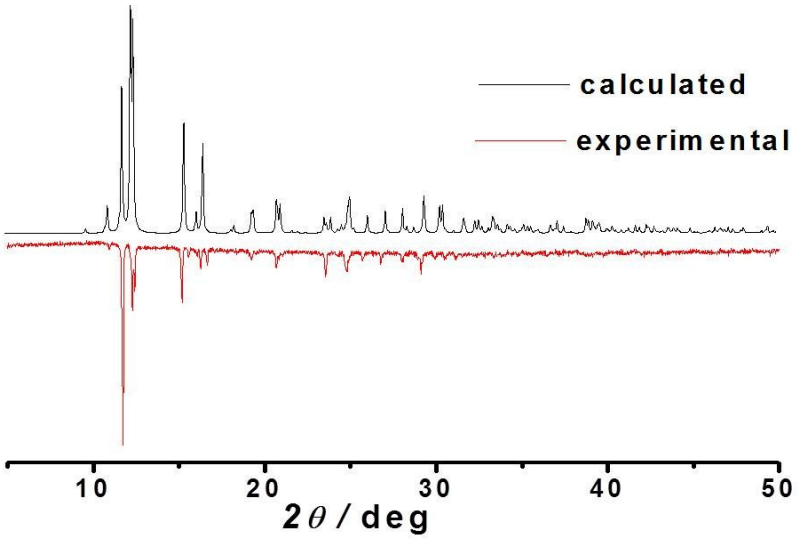

Fig. S3 XRD patterns for complex **3**.

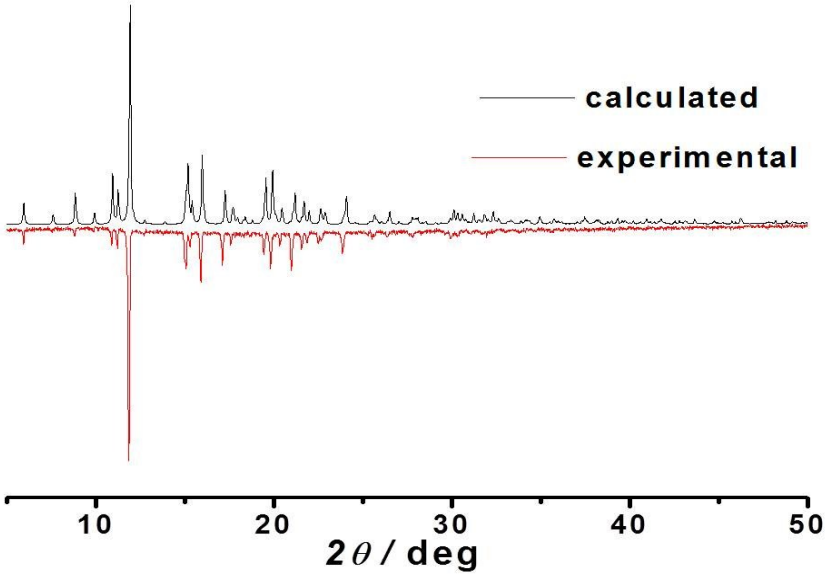

Fig. S4 XRD patterns for complex **4**.

Table S1 Summary of crystal data and refinement for **1-4**.

	1	**2**	**3**	**4**
Molecular formula	$C_{29}H_{60}Co_2N_{12}OS_4$	$C_{30}H_{59}Co_2N_{13}Se_4$	$C_{16}H_{28}CoN_{10}$	$C_{37}H_{48}BCoN_5O$
CCDC No.	1877107	1877108	1877109	1877110
Formula weight	838.99	1035.60	419.41	648.54
Temperature	155(2) K	155(2) K	155(2) K	155(2) K
Crystal system	Monoclinic	Monoclinic	Monoclinic	Monoclinic
Space group	*P* $2_1/n$	*P* $2_1/n$	*P* $2_1/n$	*P* $2_1/c$
a/Å	8.6349(9)	8.8160(6)	11.4759(19)	15.0413(7)
b/Å	30.343(3)	30.768(2)	14.976(3)	9.6313(4)
c/Å	15.6470(13)	15.7142(11)	11.4761(19)	23.5659(10)
α(°)	90	90	90	90
β(°)	104.369(3)	104.702(2)	90.840(2)	99.5000(10)
γ(°)	90	90	90	90
V/Å^3	3978.2(7)	4122.9(5)	1972.1(6)	3367.1(3)
Z	4	4	4	4
D_{calc}, g/cm^3	1.401	1.668	1.413	1.279
μ / mm^{-1}	1.085	4.375	0.894	0.547
F (000)	1776	2080	884	1380
θ range [°]	1.342/25.998	2.396/25.018	2.236/25.996	2.289/25.994
Reflns collected	31449	29345	15710	26122
R_{int}	0.0596	0.0509	0.0448	0.0377
Indep. reflns	7785	7272	3876	6576
Refns obs. [$I > 2\sigma(I)$]	6813	6283	3396	5460
Data/restr./paras	7785/3/450	7272/0/451	3876/0/248	6576/372/463
Goodness-of-fit on F^2	1.141	1.052	1.060	1.043
R_1, wR_2 [I > $2\sigma(I)$][a]	0.0437/0.1186	0.0305/0.0721	0.0295/0.0751	0.0360/0.0803
R_1, wR_2 [all data][a]	0.0534/0.1374	0.0384/0.0749	0.0362/0.0779	0.0484/0.0846

Table S2 Selected Bond Lengths (Å) and Angles (deg) for complexes **1**-**4**.

1a		**1b**	
Co1-N1	2.190(3)	Co2-N7	2.304(3)
Co1-N2	2.294(3)	Co2-N8	2.180(3)
Co1-N3	2.193(2)	Co2-N9	2.316(2)
Co1-N4	2.264(3)	Co2-N10	2.180(3)
Co1-N5	2.065(3)	Co2-N11	2.073(3)
Co1-N6	2.080(3)	Co2-N12	2.072(3)
N1-Co1-N3	146.78(9)	N8-Co2-N10	146.76(10)
N2-Co1-N4	101.60(9)	N7-Co2-N9	100.99(9)
N5-Co1-N6	84.28(11)	N11-Co2-N12	86.33(12)
N2-Co1-N5	86.09(10)	N7-Co2-N11	86.19(10)
N4-Co1-N6	89.30(10)	N9-Co2-N12	86.82(11)
C13-N5-Co1	155.5(3)	C27-N11-Co2	173.4(3)
C14-N6-Co1	149.3(3)	C28-N12-Co2	173.4(3)
2a		**2b**	
Co1-N1	2.195(3)	Co2-N5	2.304(2)
Co1-N2	2.252(3)	Co2-N6	2.174(3)
Co1-N3	2.192(3)	Co2-N7	2.307(3)
Co1-N4	2.276(3)	Co2-N8	2.161(3)
Co1-N9	2.073(3)	Co2-N11	2.081(3)
Co1-N10	2.080(3)	Co2-N12	2.083(3)
N1-Co1-N3	147.80(10)	N6-Co2-N8	147.67(10)
N2-Co1-N4	101.90(10)	N5-Co2-N7	101.54(9)
N9-Co1-N10	83.85(11)	N11-Co2-N12	85.88(11)

N2-Co1-N10	89.14(10)	N5-Co2-N12	86.85(10)
N4-Co1-N9	86.42(10)	N7-Co2-N11	85.83(10)
C25-N9-Co1	153.2(3)	C27-N11-Co2	175.1(3)
C26-N10-Co1	155.4(3)	C28-N12-Co2	175.3(3)

3		**4**	
Co1-N1	2.2731(13)	Co1-N1	2.108(3)
Co1-N2	2.1762(14)	Co1-N2	2.161(4)
Co1-N3	2.2826(13)	Co1-N3	2.169(7)
Co1-N4	2.1791(14)	Co1-N4	2.205(3)
Co1-N5	2.1058(14)	Co1-N5	1.9399(17)
Co1-N8	2.0756(15)	N1-Co1-N2	82.33(10)
N2-Co1-N4	147.78(5)	N1-Co1-N4	82.68(10)
N1-Co1-N3	102.29(5)	N2-Co1-N3	82.48(14)
N5-Co1-N8	83.38(6)	N1-Co1-N3	136.0(2)
N1-Co1-N5	86.75(5)	N2-Co1-N4	136.71(13)
N3-Co1-N8	88.03(5)	N3-Co1-N4	80.88(14)
C13-N5-Co1	163.20(15)	N1-Co1-N5	117.12(10)
C15-N8-Co1	160.01(14)	N2-Co1-N5	106.84(11)
C14-N6-C13	123.64(17)	N3-Co1-N5	106.70(2)
C16-N9-C15	119.12(15)	N4-Co1-N5	116.16(10)

Table S3 The results of the continuous shape measures (*CShMs*) analyses of **1**, **2**, **3** and **4** by SHAPE software[S1]

CShM		**1a**	**1b**	**2a**	**2b**	**3**
Six-vertex	Hexagon	33.971	33.631	33.757	33.517	33.729
	Pentagonal pyramid	19.098	19.191	19.173	19.166	18.840

	Octahedron	3.277	2.760	3.230	2.659	2.967
	Trigonal prism	6.603	8.094	6.578	8.566	7.589
	Johnson pentagonal pyramid	22.939	22.985	22.998	22.914	22.627

CShM		**4**
Five-vertex	Pentagon	31.087
	Vacant octahedron	3.468
	Trigonal bipyramid	5.661
	Spherical square pyramid	0.442
	Johnson trigonal bipyramid	8.642

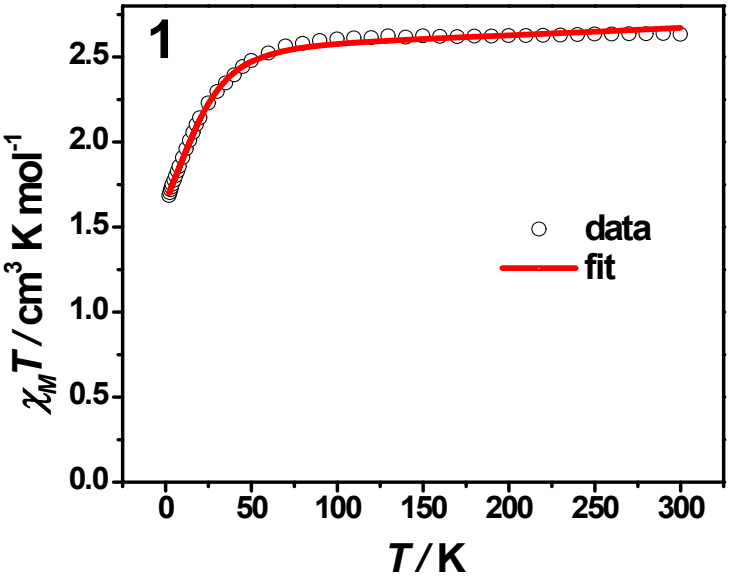

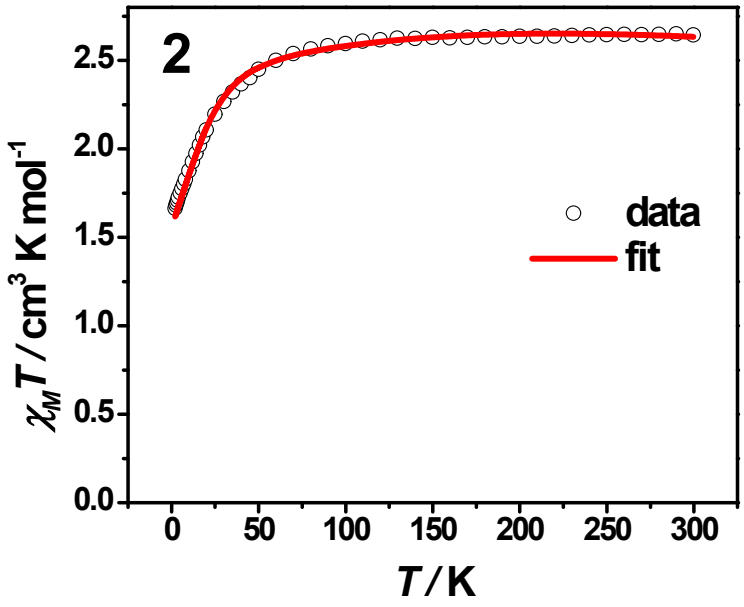
2
data
fit
$\chi_M T$ / cm^3 K mol^{-1}
T / K
0.0
0.5
1.0
1.5
2.0
2.5
0
50
100
150
200
250
300

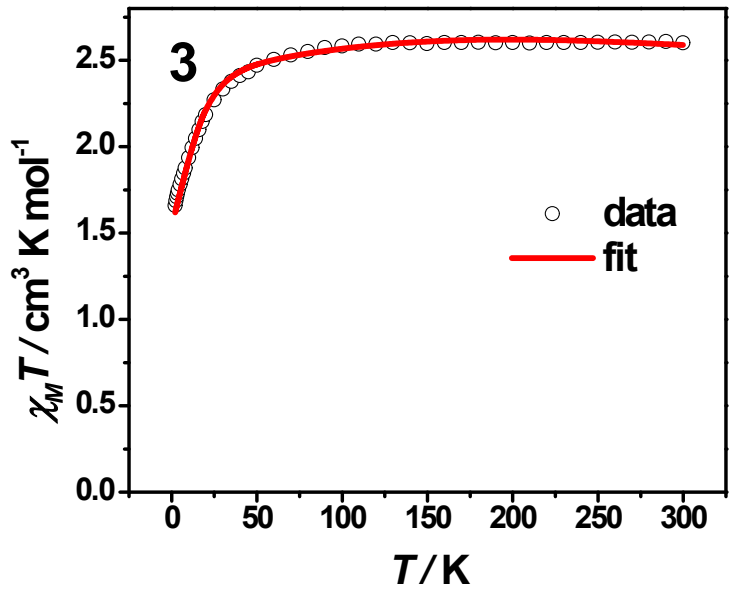
3
data
fit
$\chi_M T$ / cm^3 K mol^{-1}
T / K
0.0
0.5
1.0
1.5
2.0
2.5
0
50
100
150
200
250
300

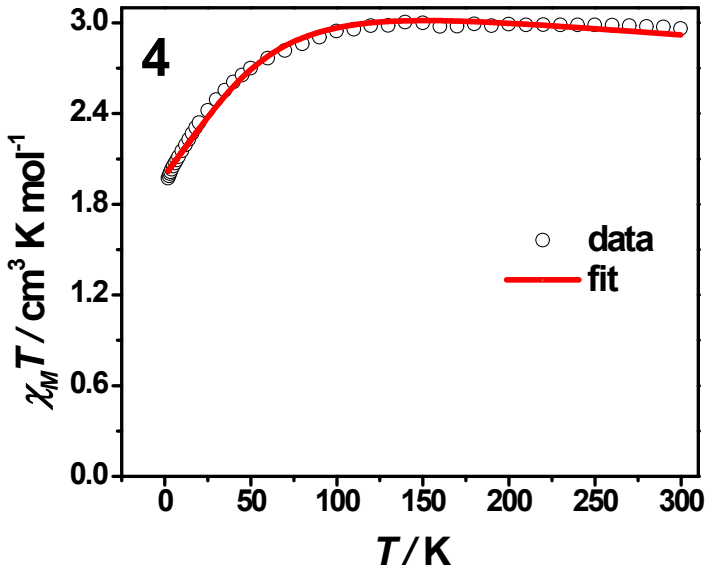

Fig. S5 Variable-temperature dc susceptibility data under 0.1 T applied dc field of **1**, **2, 3** and **4**. Solid lines are the fits to the data using the full Hamiltanian as shown eqn (1) with the program *PHI*[S2].

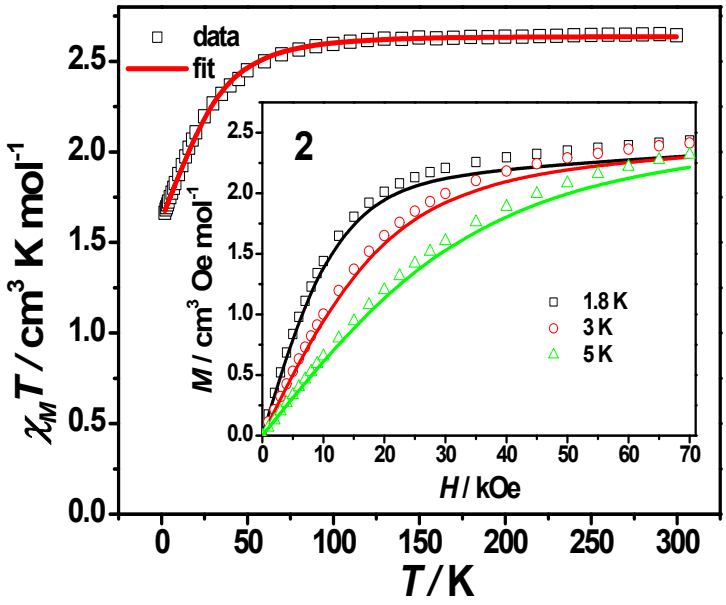

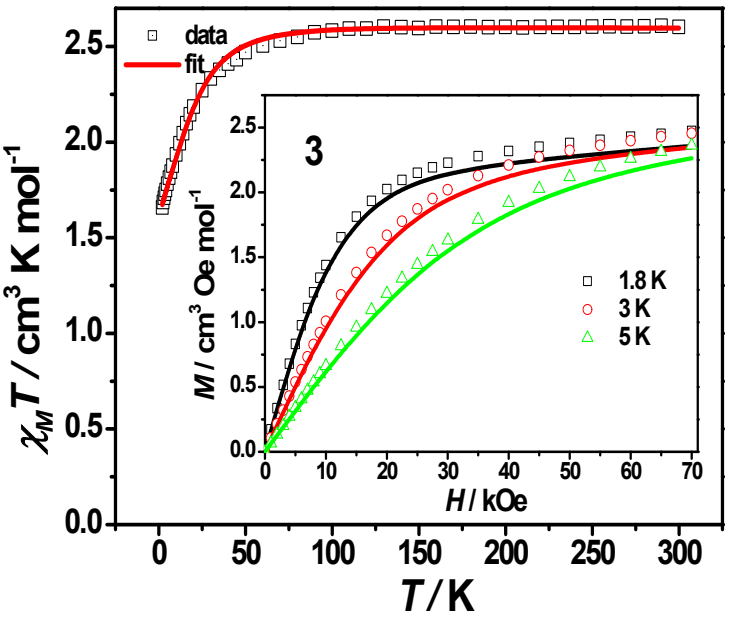

Fig. S6 Variable-temperature dc susceptibility data under 0.1 T applied dc field of **2** and **3**. Inset: field dependence of the magnetization below 5 K. Solid lines are the fits to the magnetic data using the spin Hamiltanian as shown in eqn (2) with the program *PHI*[S2].

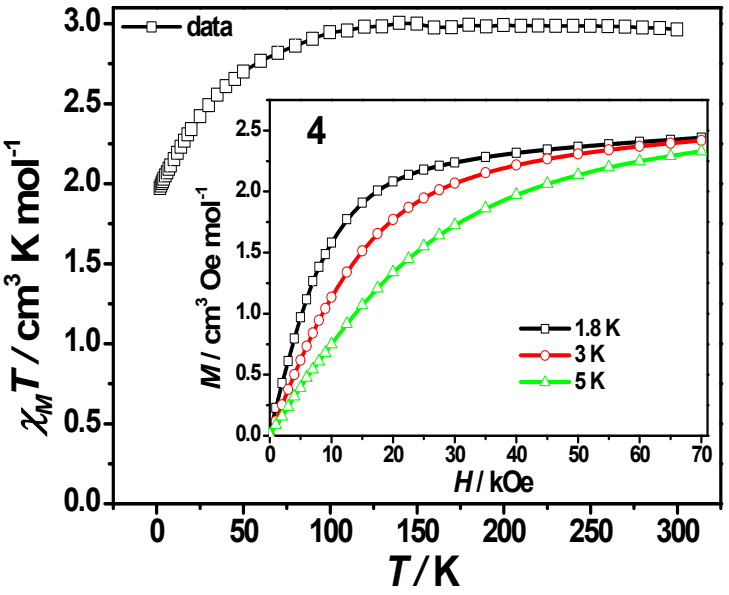

Fig. S7 Variable-temperature dc susceptibility data under 0.1 T applied dc field of **4**. Inset: field dependence of the magnetization below 5 K. The solid lines are for eye guide.

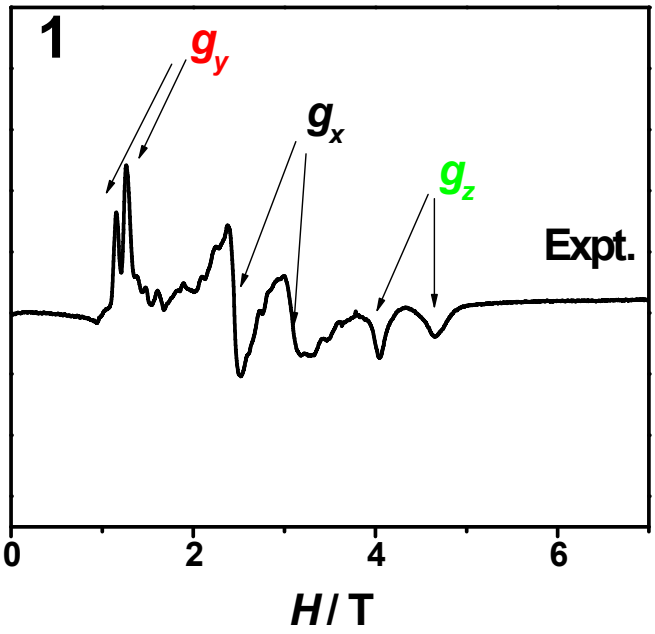

Fig. S8 The experimental spectra for complex **1** with g_y = 6.37 and 5.76, g_x = 2.93 and 2.34, g_z = 1.79 and 1.55 under 106 GHz in derivative mode at 4.2 K.

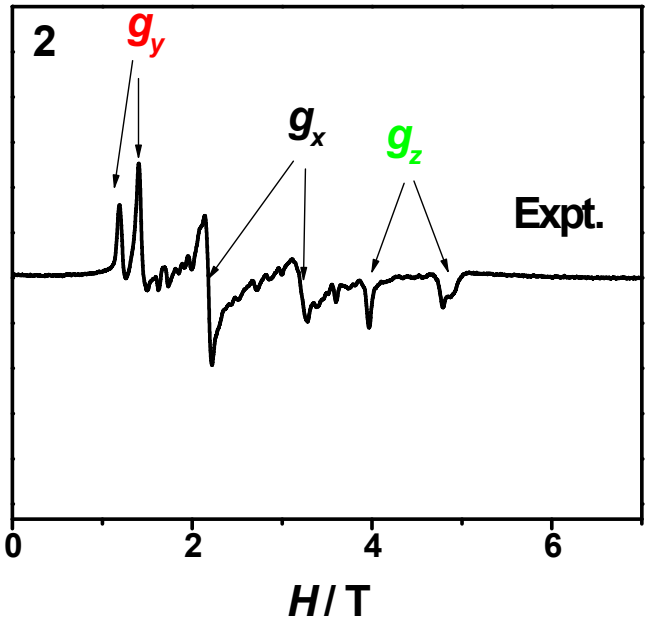

Fig. S9 The experimental spectra for complex **2** with g_y = 6.42 and 5.41, g_x = 3.46 and 2.37, g_z = 1.91 and 1.57 under 112 GHz in derivative mode at 4.2 K.

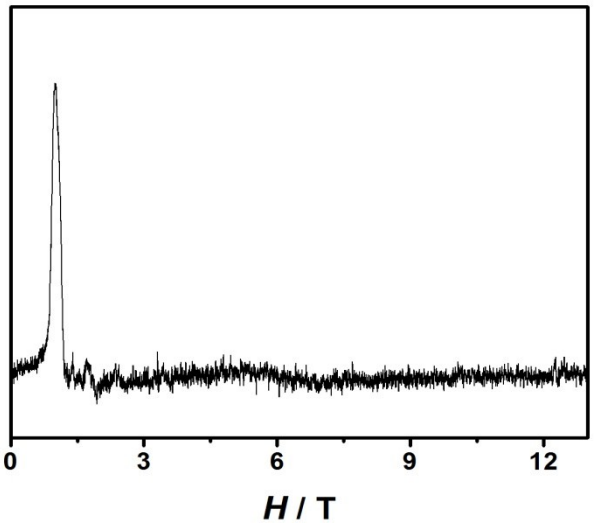

Fig. S10 The HEFER spectrum for complex **4** under 112 GHz at 4.2 K.

Computational details

Both of complexes **1** and **2** have two types of structures **1a** and **1b** for **1**, and **2a** and **2b** for **2**. Complete active space second-order multiconfigurational perturbation theory (CASPT2) considering the effect of the dynamic electron correlation based on complete-active-space self-consistent field (CASSCF) method with MOLCAS 8.2 program package[S4] was performed on (see Fig. S11 for the calculated complete structure of **1a**; see Fig. S14 for the other complete structures) the basis of single-crystal X-ray determined geometries of **1**−**4**. For the first CASSCF calculation, the basis sets for all atoms are atomic natural orbitals from the MOLCAS ANO-RCC library: ANO-RCC-VTZP for magnetic center ion Co^{II}; VTZ for close N atoms; VDZ for distant atoms. The calculations employed the second order Douglas-Kroll-Hess Hamiltonian, where scalar relativistic contractions were taken into account in the basis set. The effect of the dynamical electronic correlation was applied using CASPT2 based on the first CASSCF calculation. After that, the spin-orbit coupling was handled separately in the restricted active space state interaction (RASSI-SO) procedure. For all complexes, the active electrons in 5+5′ active spaces include all *d* electrons (CAS(7 in 5+5′)) in the CASSCF calculations. To exclude all the doubts, we calculated all the roots in the active space. We have mixed the maximum number of spin-free state which was possible with our hardware (all from 10 quadruplets and 20 from 40 doublets). Single_Aniso[S5] program was used to obtain zero-field splitting parameters D (E) (cm^{-1}), $\boldsymbol{g}$ tensors, energy levels, magnetic axes, *et al.,* based on the above CASPT2/RASSI calculations.

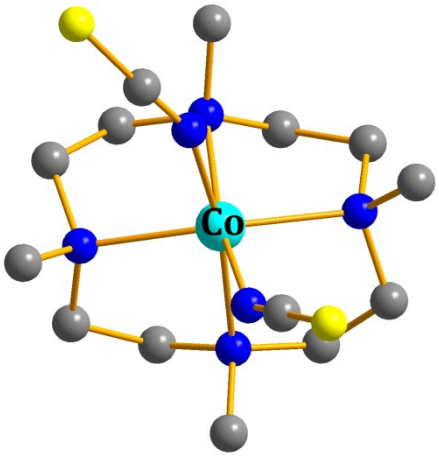

Fig. S11 Calculated complete structure of **1a**. H atoms are omitted for clarity.

Table S4 Calculated spin-free energies (cm^{-1}) of the lowest ten terms (S = 3/2) of complexes **1**−**4** using CASPT2/RASSI with MOLCAS 8.2.

spin-free states	**1a**	**1b**	**2a**	**2b**	**3**	**4**
	E/cm^{-1}	E/cm^{-1}	E/cm^{-1}	E/cm^{-1}	E/cm^{-1}	E/cm^{-1}
1	0.0	0.0	0.0	0.0	0.0	0.0
2	1516.0	1565.3	1440.1	1556.9	1687.2	375.7
3	2667.9	2530.8	2502.3	2442.3	2614.7	1306.5
4	7735.5	7849.3	7784.1	8041.1	8069.0	3095.4
5	8481.3	8458.3	8608.4	8503.8	8577.8	7620.8
6	9336.3	9232.8	9314.2	9213.5	9355.8	7973.2
7	16692.2	16854.7	16838.4	16925.9	17043.9	10720.3
8	20212.2	20146.9	20743.8	20772.4	20424.7	17326.4
9	20704.8	21766.5	21178.1	21241.8	20850.1	17906.7
10	21707.3	12250.8	22123.3	21962.8	21486.3	19138.7

Table S5. Calculated weights of the five most important spin-free states for the lowest two spin-orbit states of complexes **1**−**4** using CASPT2/RASSI with MOLCAS 8.2.

	Spin-orbit states	Energy (cm^{-1})	Spin-free states, Spin, Weights				
1a	1	0.0	1, 1.5, 0.9260	2, 1.5, 0.0615	3, 1.5, 0.0095	5, 1.5, 0.0009	4, 1.5, 0.0008
	2	61.3	1, 1.5, 0.9756	2, 1.5, 0.0113	3, 1.5, 0.0063	4, 1.5, 0.0034	5, 1.5, 0.0016
1b	1	0.0	1, 1.5, 0.9292	2, 1.5, 0.0564	3, 1.5, 0.0114	5, 1.5, 0.0010	4, 1.5, 0.0007
	2	56.5	1, 1.5, 0.9754	2, 1.5, 0.0115	3, 1.5, 0.0063	4, 1.5, 0.0034	5, 1.5, 0.0016
2a	1	0.0	1, 1.5, 0.9217	2, 1.5, 0.0628	3, 1.5, 0.0126	5, 1.5, 0.0010	4, 1.5, 0.0007
	2	62.8	1, 1.5, 0.9727	2, 1.5, 0.0134	3, 1.5, 0.0073	4, 1.5, 0.0034	5, 1.5, 0.0014
2b	1	0.0	1, 1.5, 0.9299	2, 1.5, 0.0514	3, 1.5, 0.0158	5, 1.5, 0.0011	4, 1.5, 0.0005
	2	54.8	1, 1.5, 0.9729	2, 1.5, 0.0142	3, 1.5, 0.0065	4, 1.5, 0.0033	5, 1.5, 0.0014
3	1	0.0	1, 1.5, 0.9382	2, 1.5, 0.0478	3, 1.5, 0.0109	5, 1.5, 0.0011	4, 1.5, 0.0006
	2	51.4	1, 1.5, 0.9769	2, 1.5, 0.0105	3, 1.5, 0.0062	4, 1.5, 0.0032	5, 1.5, 0.0014
4	1	0.0	1, 1.5, 0.6853	2, 1.5, 0.2837	3, 1.5, 0.0218	4, 1.5, 0.0066	5, 1.5, 0.0005
	2	162.3	1, 1.5, 0.8444	2, 1.5, 0.0827	3, 1.5, 0.0649	4, 1.5, 0.0038	5, 1.5, 0.0011

Table S6. Calculated zero-field splitting parameters D (E) (cm^{-1}) and $\boldsymbol{g}$ (g_x, g_y, g_z) tensors of the lowest spin-orbit state of complexes **1**−**3** using CASPT2/RASSI with MOLCAS 8.2.

	1a	**1b**	**2a**	**2b**
CAS	(7, 5+5′)	(7, 5+5′)	(7, 5+5′)	(7, 5+5′)
*S*pin	S_{Co} = 3/2	S_{Co} = 3/2	S_{Co} = 3/2	S_{Co} = 3/2
D(E)	26.6(8.8)	24.5(8.1)	27.4(8.9)	25.9(−5.2)
$\boldsymbol{g}$	2.545 2.296 2.135	2.516 2.274 2.117	2.542 2.283 2.112	2.499 2.313 2.111

	3
CAS	(7, 5+5′)
Spin	S_{Co} = 3/2
D(E)	22.5(7.2)
$\boldsymbol{g}$	2.484 2.271 2.116

Table S7 Calculated energy levels (cm^{-1}), $\boldsymbol{g}$ (g_x, g_y, g_z) tensors of the lowest two doublets (S = 1/2) of complex **4** using CASPT2/RASSI with MOLCAS 8.2.

	E/cm^{-1}	$\boldsymbol{g}$
1	0.0	0.541 0.735 9.253
2	162.3	4.462 4.008 3.381

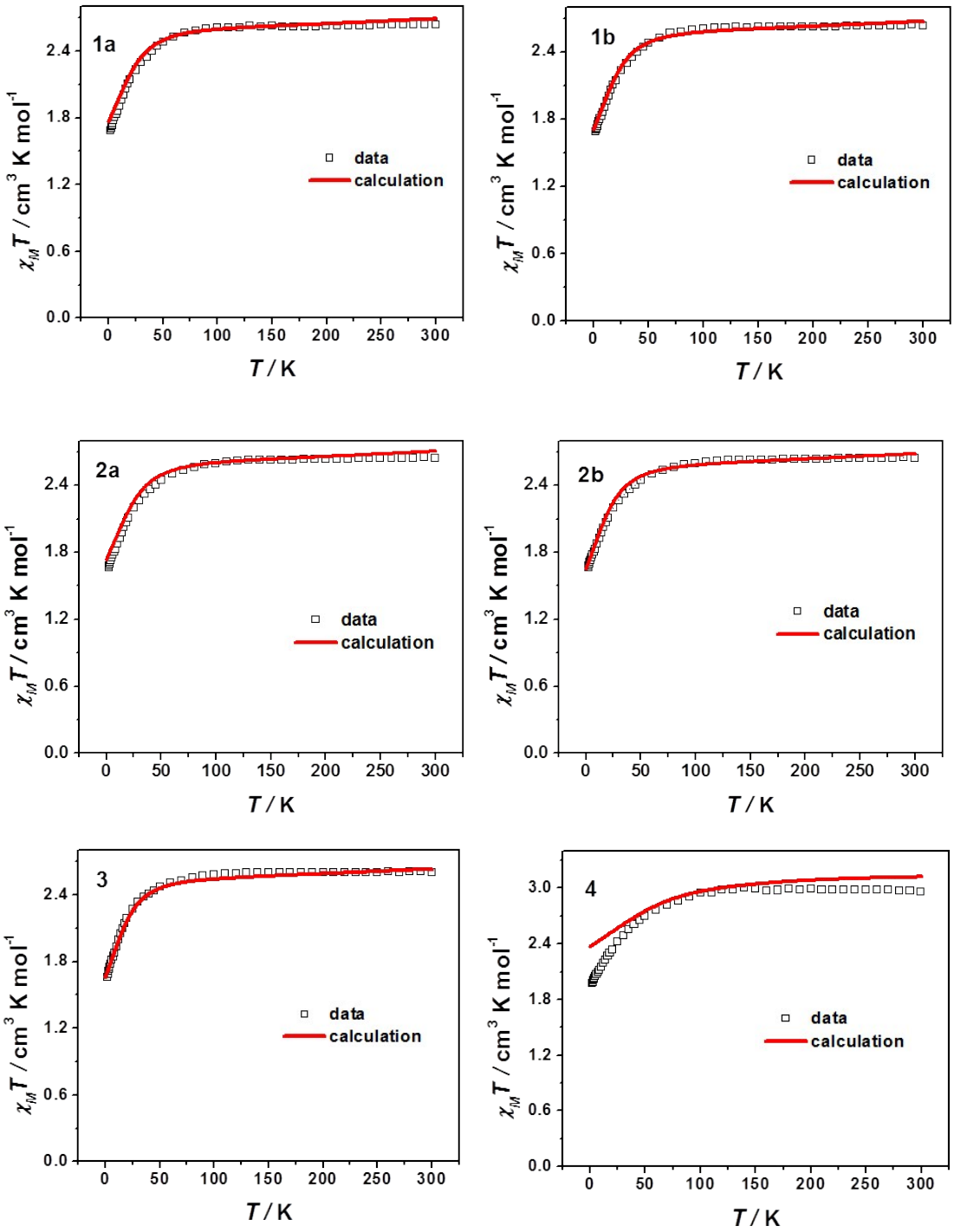

Fig. S12 The theoretical (red solid line) curves of magnetic susceptibilities of **1a**, **1b**, **2a**, **2b**, **3** and **4** compared with the experimental data.

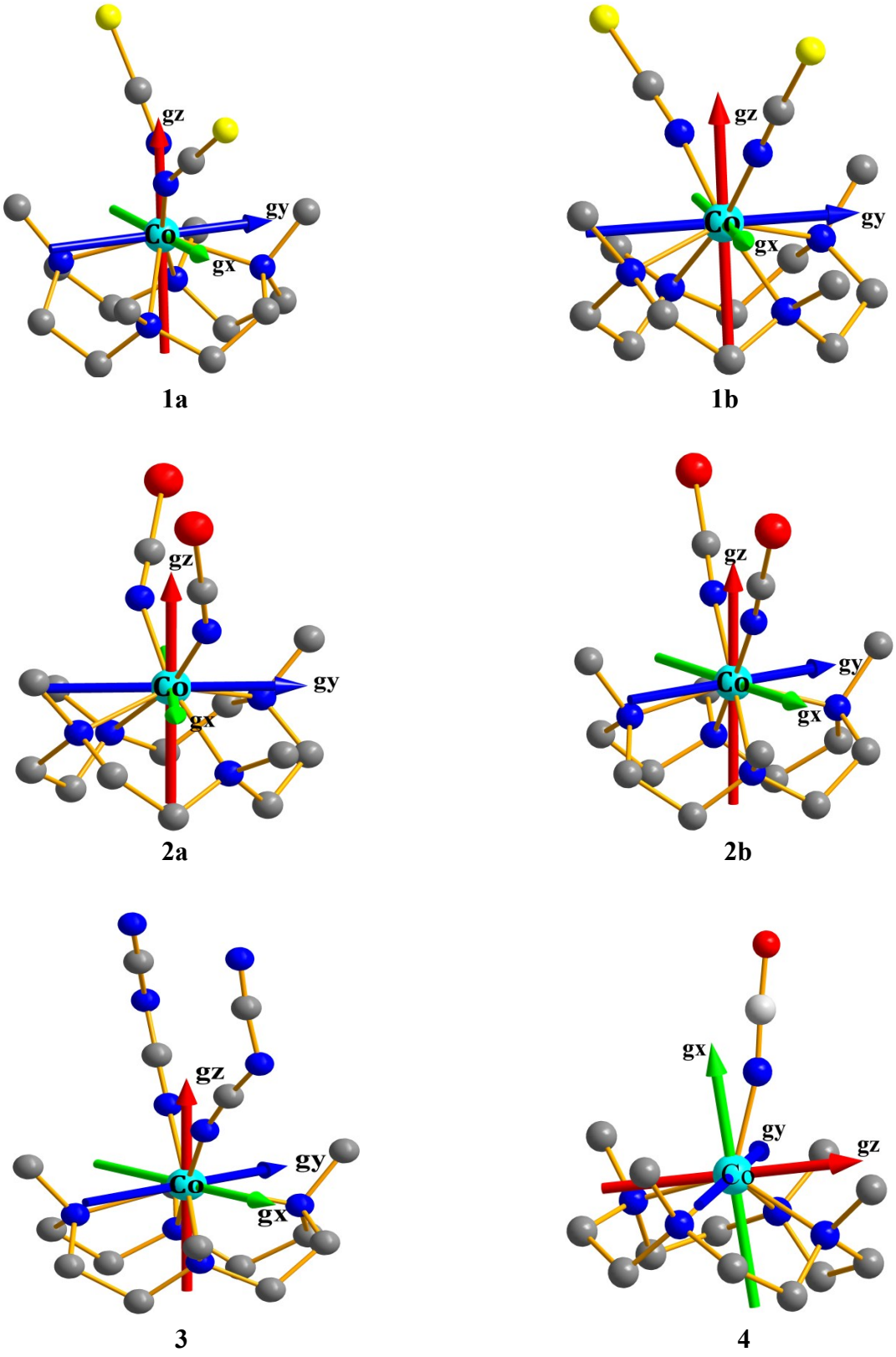

Fig. S13 Calculated orientations of the local main magnetic axes (g_x: green; g_y: blue; g_z: red) on Co^{II} ions of **1a**, **1b**, **2a**, **2b**, **3** and **4**.

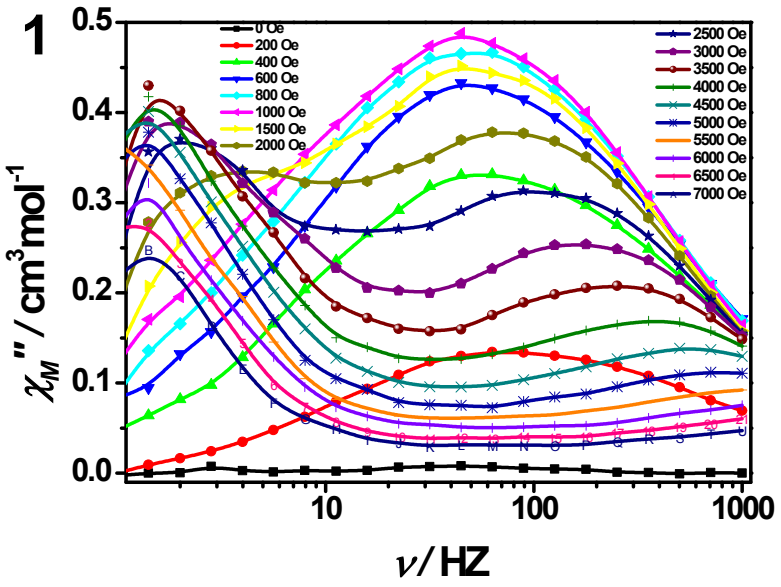
1
0 Oe
200 Oe
400 Oe
600 Oe
800 Oe
1000 Oe
1500 Oe
2000 Oe
2500 Oe
3000 Oe
3500 Oe
4000 Oe
4500 Oe
5000 Oe
5500 Oe
6000 Oe
6500 Oe
7000 Oe
0.0
0.1
0.2
0.3
0.4
0.5
10
100
1000
χM" / cm3mol-1
ν / HZ

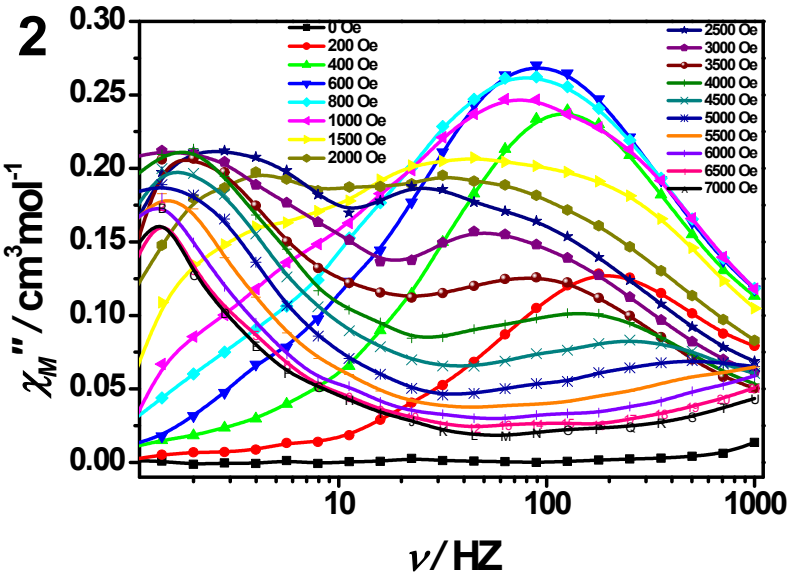
2
0 Oe
200 Oe
400 Oe
600 Oe
800 Oe
1000 Oe
1500 Oe
2000 Oe
2500 Oe
3000 Oe
3500 Oe
4000 Oe
4500 Oe
5000 Oe
5500 Oe
6000 Oe
6500 Oe
7000 Oe
0.00
0.05
0.10
0.15
0.20
0.25
0.30
10
100
1000
χM" / cm3mol-1
ν / HZ

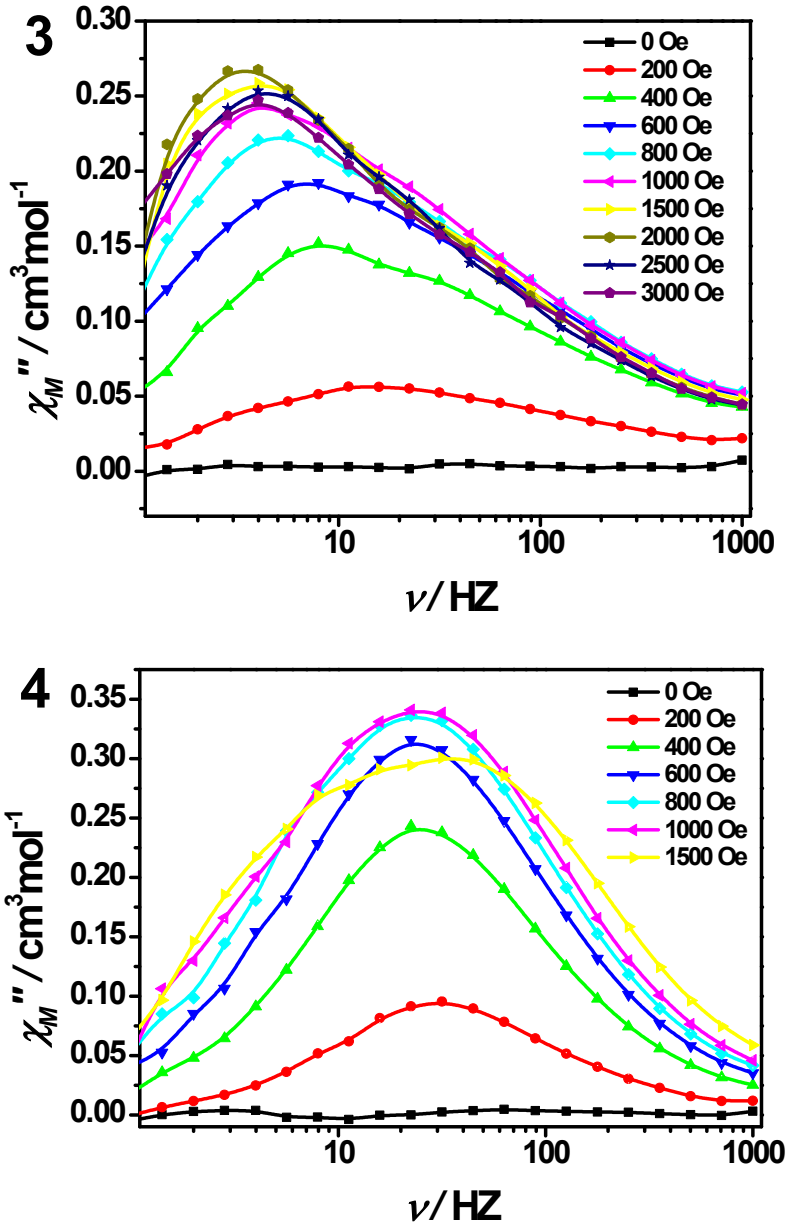

Fig. S14 Frequency dependence of out-of-phase (χ_M'') ac susceptibility at 1.8 K under the different applied static fields for **1**, **2**, **3** and **4**. The solid lines are for eye guide.

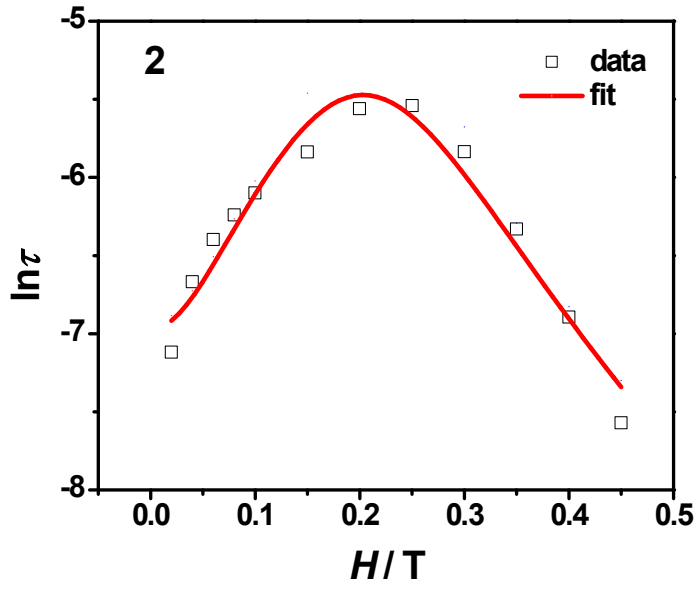
2
data
fit
-5
-6
-7
-8
lnτ
0.0
0.1
0.2
0.3
0.4
0.5
H / T

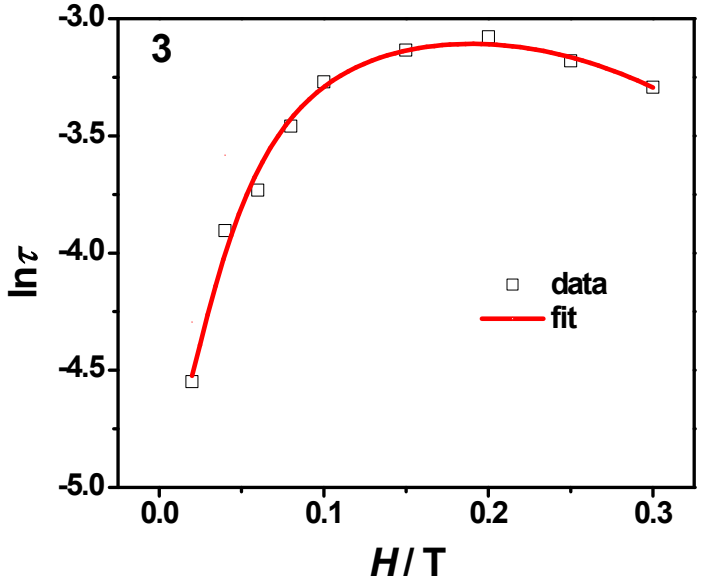
3
data
fit
-3.0
-3.5
-4.0
-4.5
-5.0
lnτ
0.0
0.1
0.2
0.3
H / T

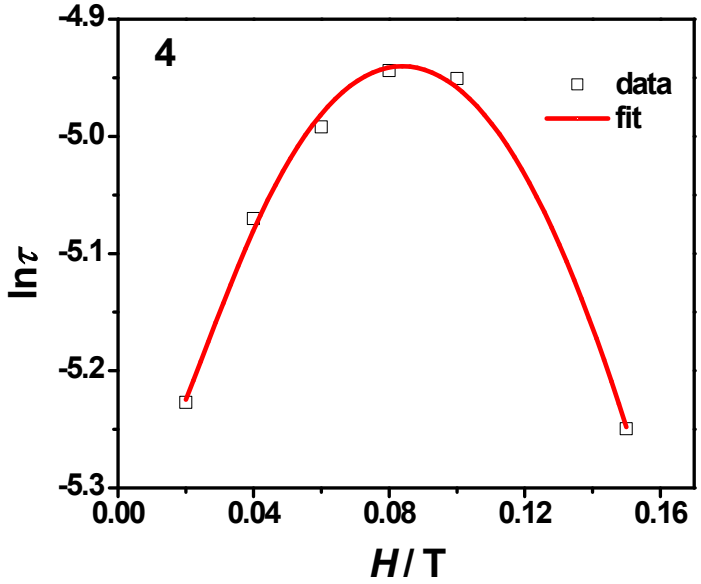

Fig. S15 Field dependence of the magnetization relaxation times for **2**, **3** and **4**. The red line represents the best fit by using eqn (3).

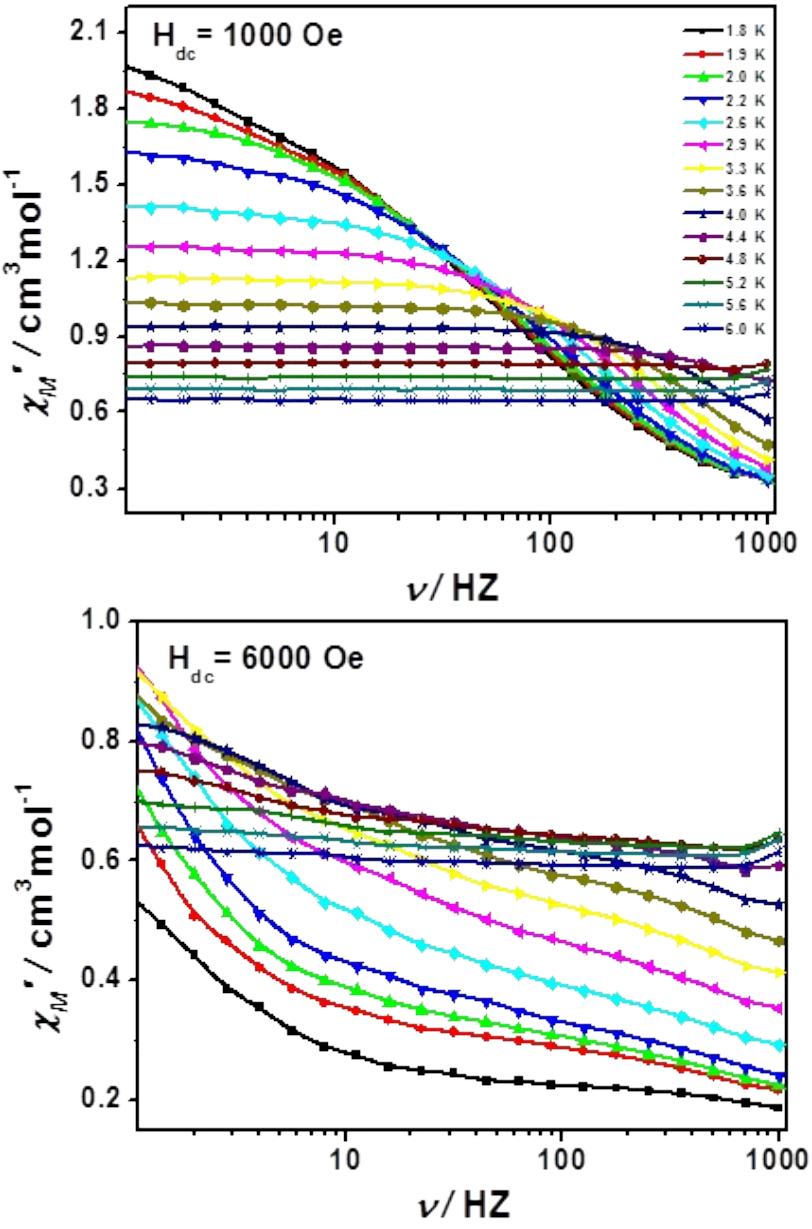

Fig. S16 Frequency dependence of in-of-phase (χ_M') ac susceptibility from 1.8 to 6 K for **1** under 0.1 T and 0.6 T, respectively. The solid lines are for eye guide.

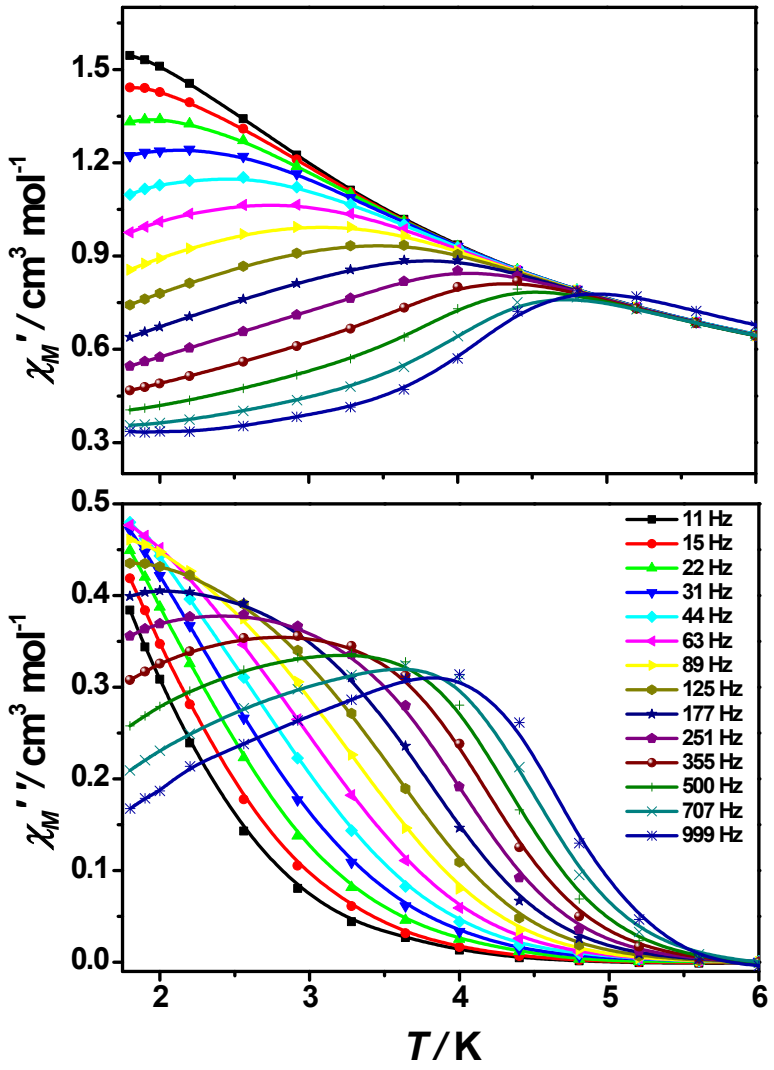

Fig. S17 Temperature dependence of in-of-phase (χ_M') and out-of-phase ac susceptibility (χ_M'') at different ac frequency under a 0.1 T dc field for **1**. The solid lines are for eye guide.

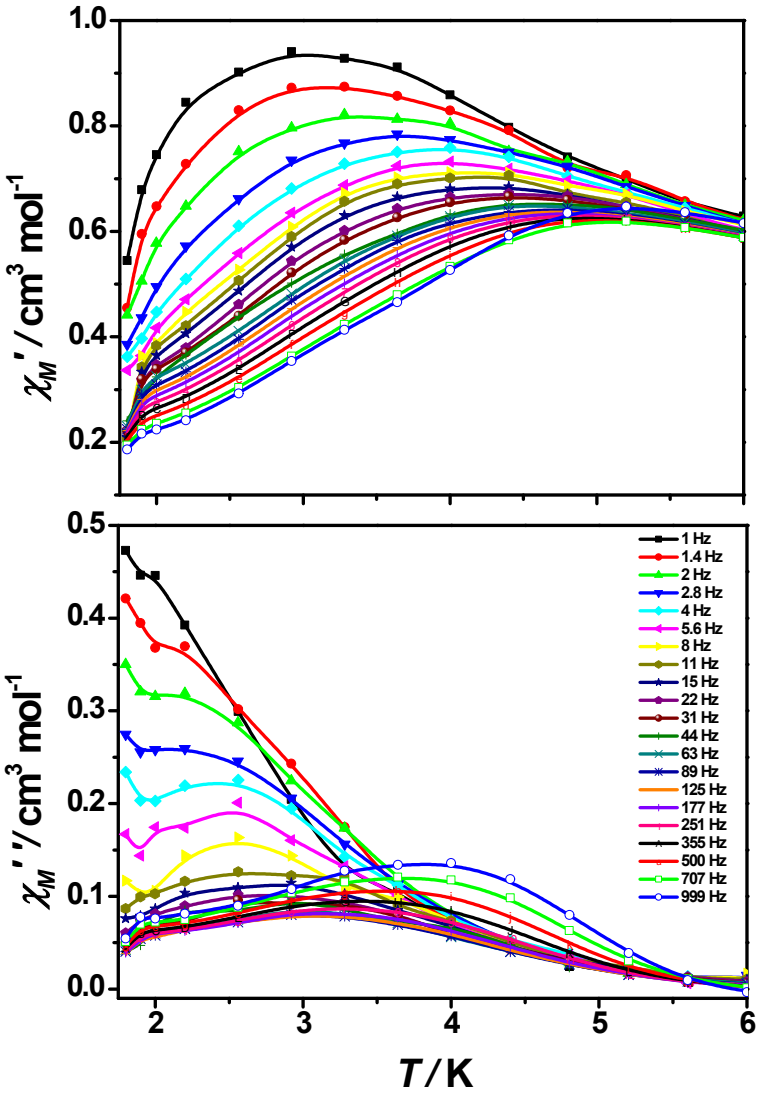

Fig. S18 Temperature dependence of in-of-phase (χ_M') and out-of-phase ac susceptibility (χ_M'') at different ac frequency under a 0.6 T dc field for **1**. The solid lines are for eye guide.

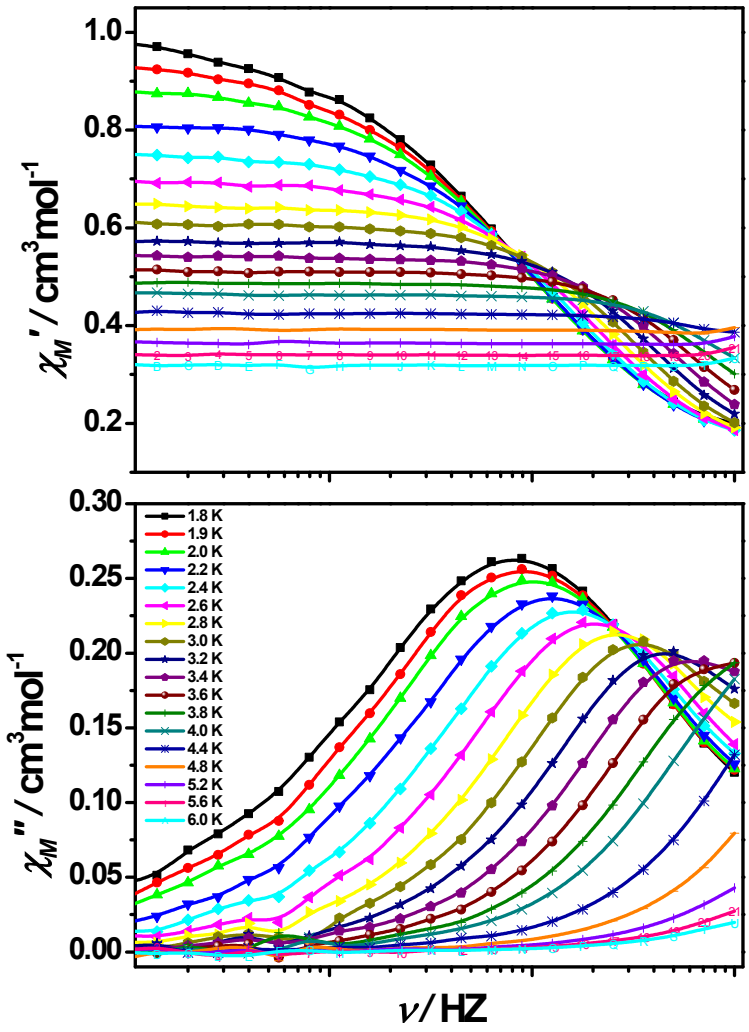

Fig. S19 Frequency dependence of the ac susceptibility from 1.8 to 6 K for **2** under 0.08 T. The solid lines are for eye guide.

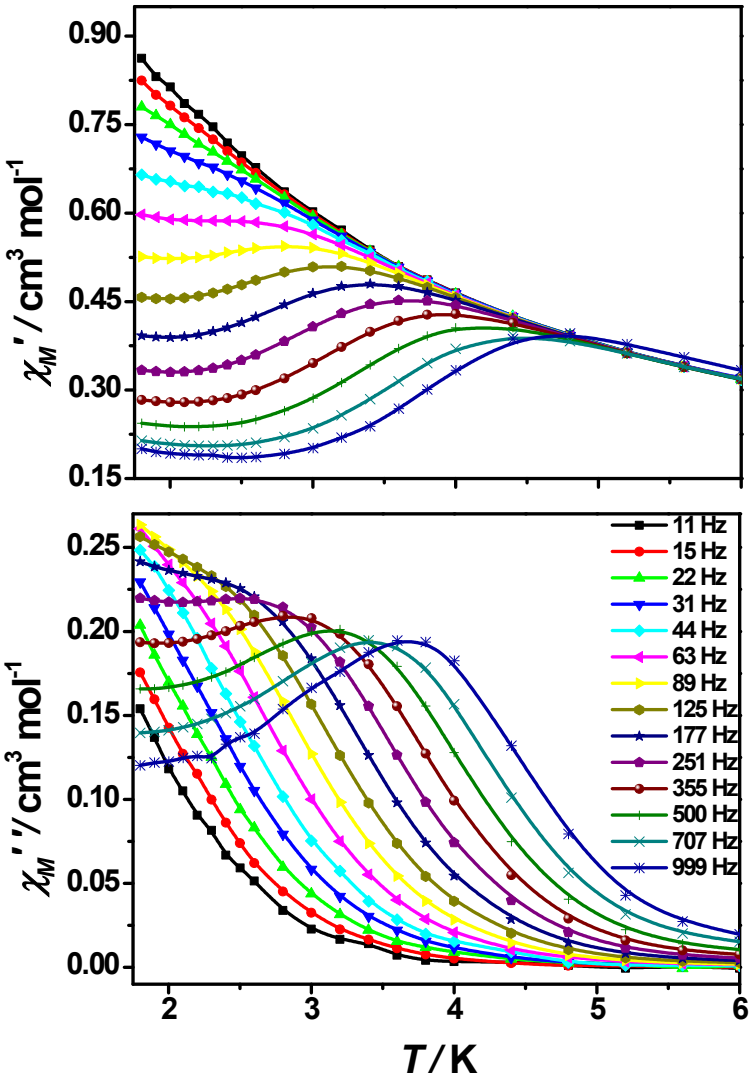

Fig. S20 Temperature dependence of in-of-phase (χ_M') and out-of-phase ac susceptibility (χ_M'') at different ac frequency under a 0.08 T dc field for **2**. The solid lines are for eye guide.

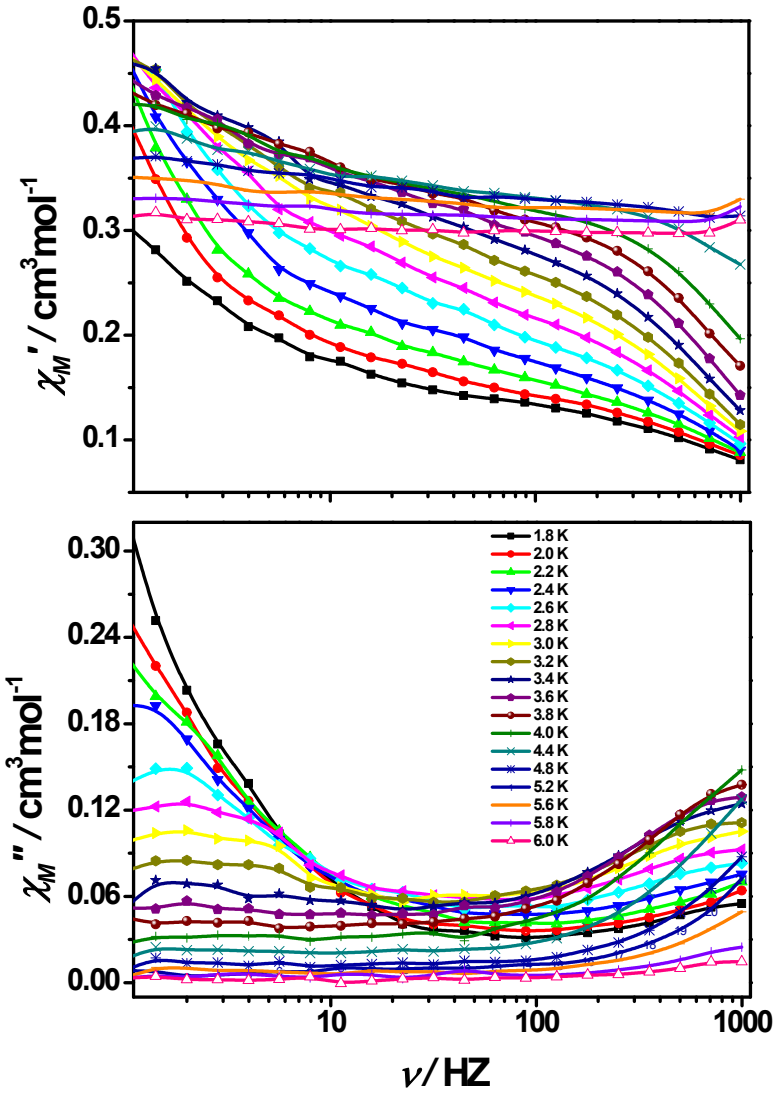

Fig. 21 Frequency dependence of the ac susceptibility from 1.8 to 6 K for **2** under 0.6 T. The solid lines are for eye guide.

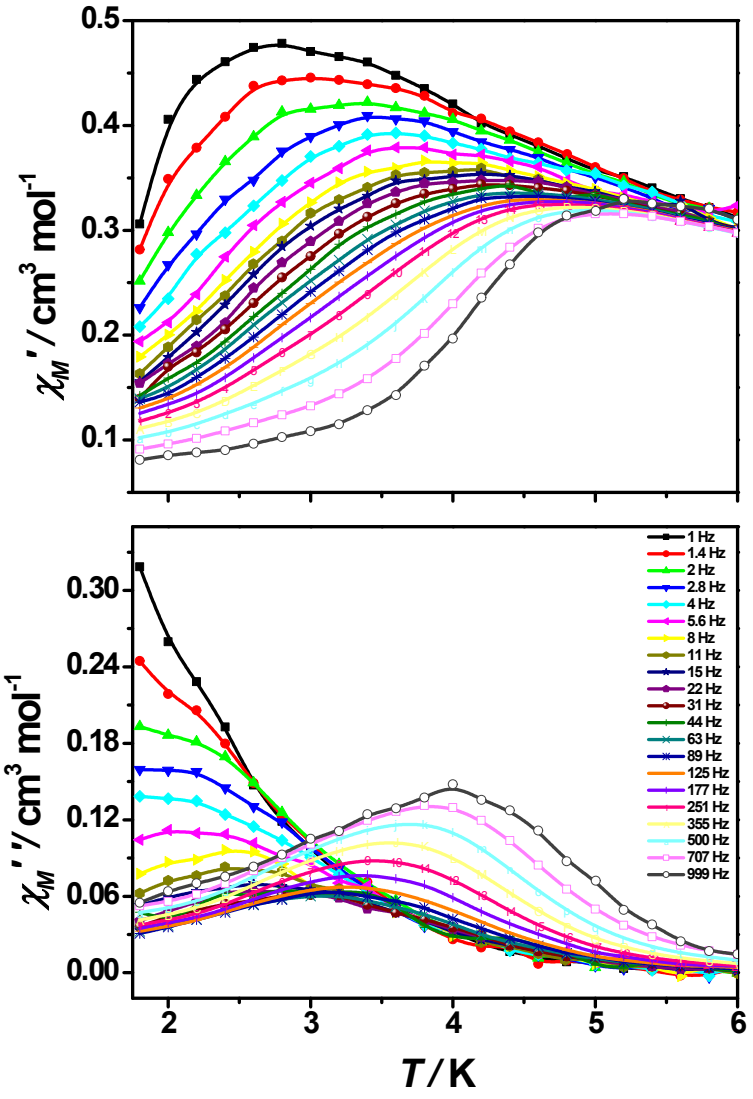

Fig. S22 Temperature dependence of in-of-phase (χ_M') and out-of-phase ac susceptibility (χ_M'') at different ac frequency under a 0.6 T dc field for **2**. The solid lines are for eye guide.

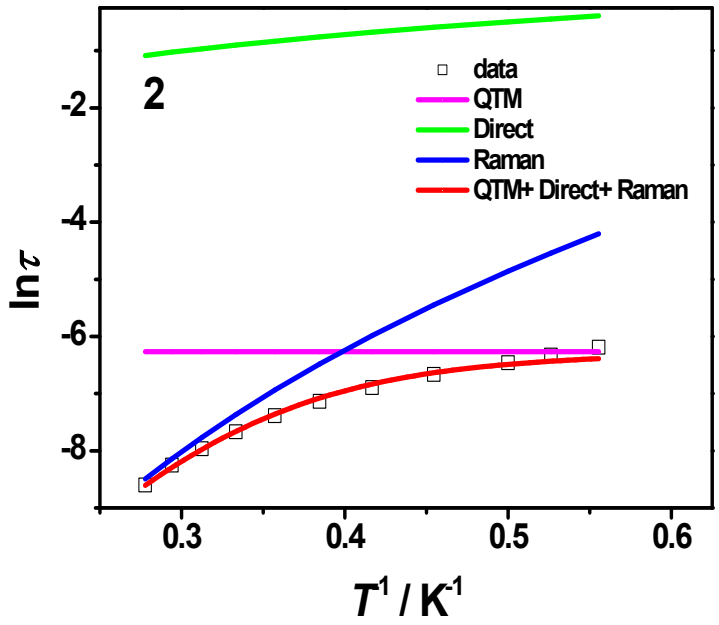

Fig. S23 Relaxation time of the magnetization *ln(τ)* vs T^{-1} plots for **2** at 0.08 T.

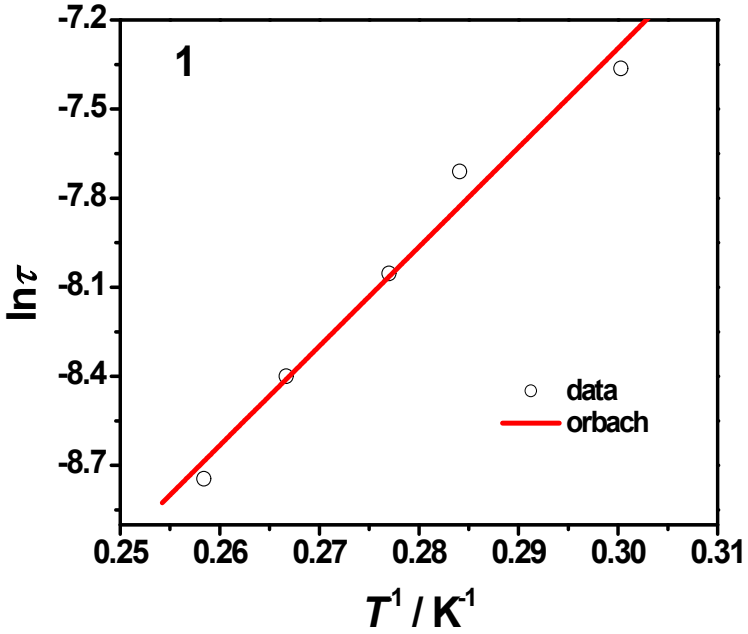

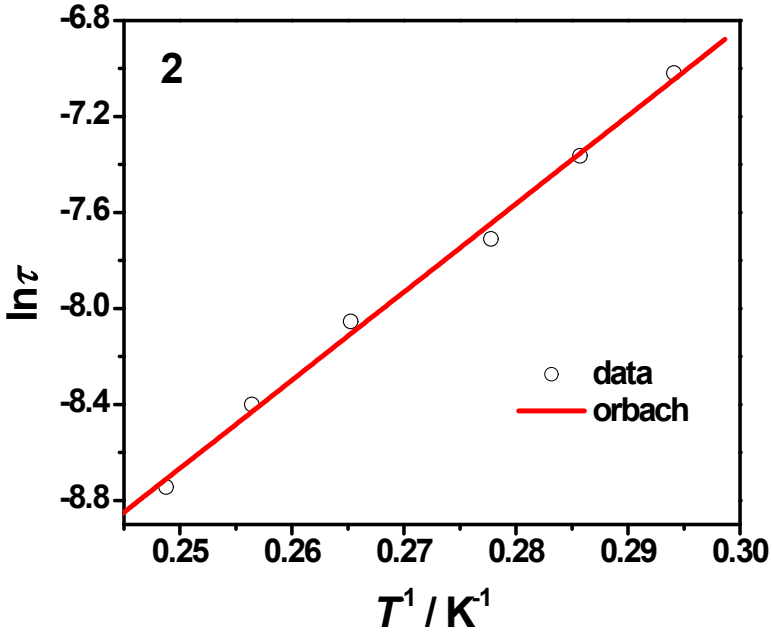

Fig. S24 Relaxation time of the magnetization *ln(τ)* vs T^{-1} plots for **1**-**2** at 0.6 T fitted with Arrhenius' law $\tau = \tau^0 \exp(U_{eff}/k_BT)$.

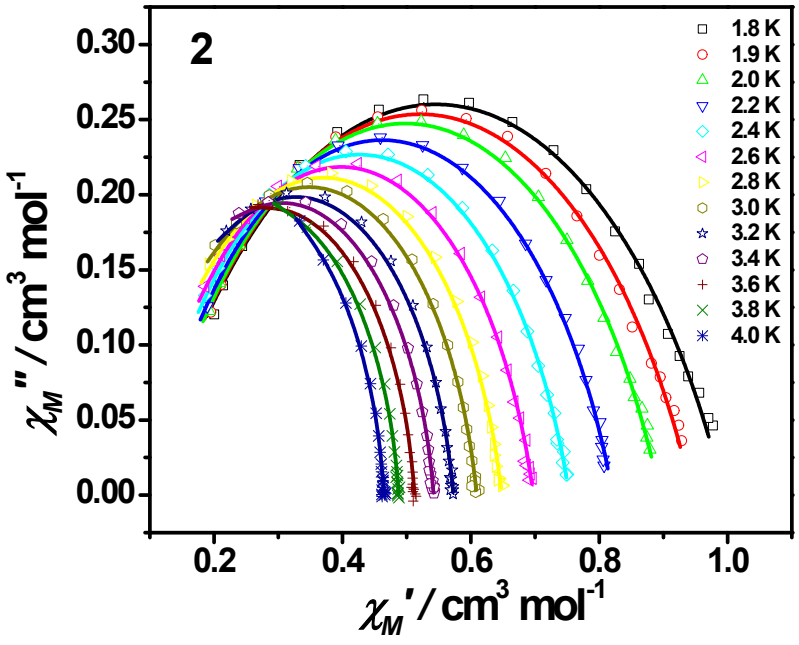

Fig. S25 Cole-Cole plot obtained from the ac susceptibility data under different range of temperature for **2**. Solid lines represent the best fits to a generalized Debye model[S6].

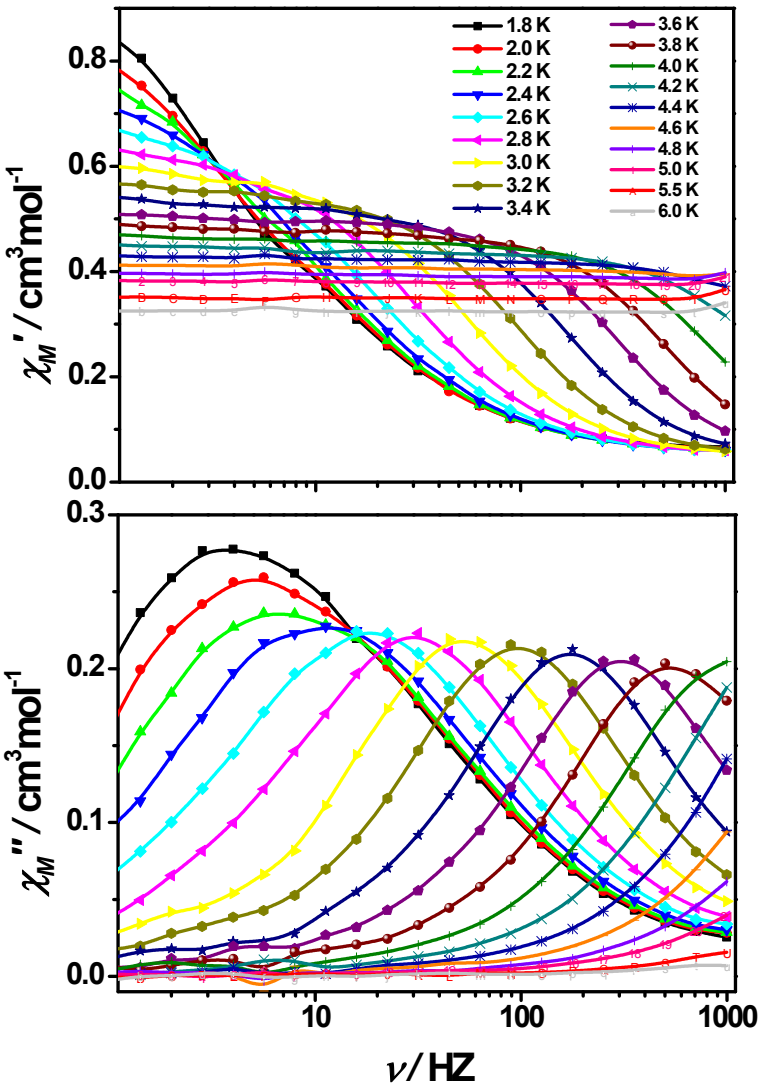

Fig. S26 Frequency dependence of the ac susceptibility from 1.8 to 6 K for **3** under 0.2 T. The solid lines are for eye guide.

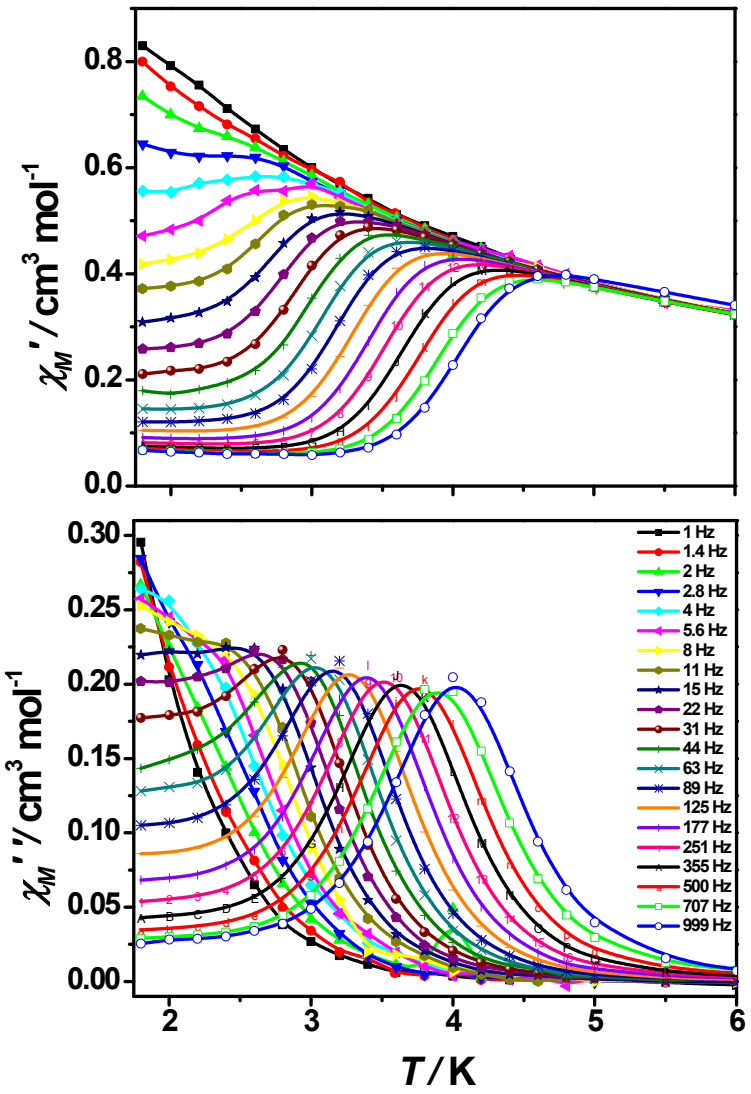

Fig. S27 Temperature dependence of in-of-phase (χ_M') and out-of-phase ac susceptibility (χ_M'') at different ac frequency under a 0.2 T dc field for **3**. The solid lines are for eye guide.

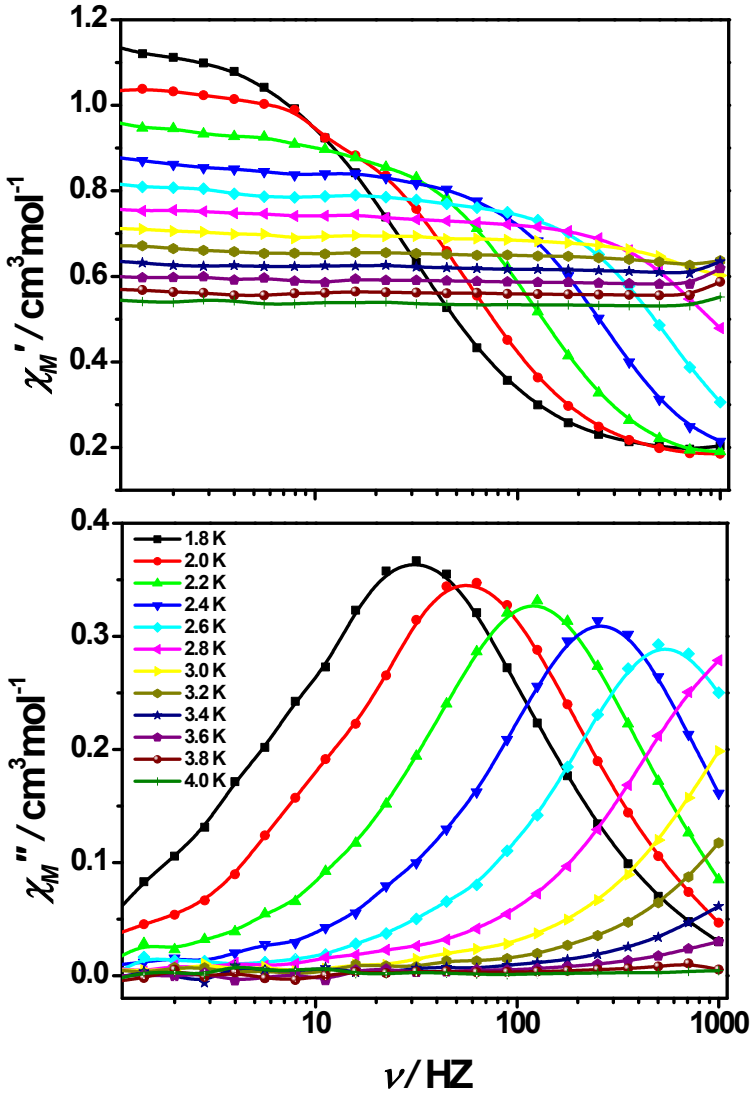

Fig. S28 Frequency dependence of the ac susceptibility from 1.8 to 4 K for **4** under 0.1 T. The solid lines are for eye guide.

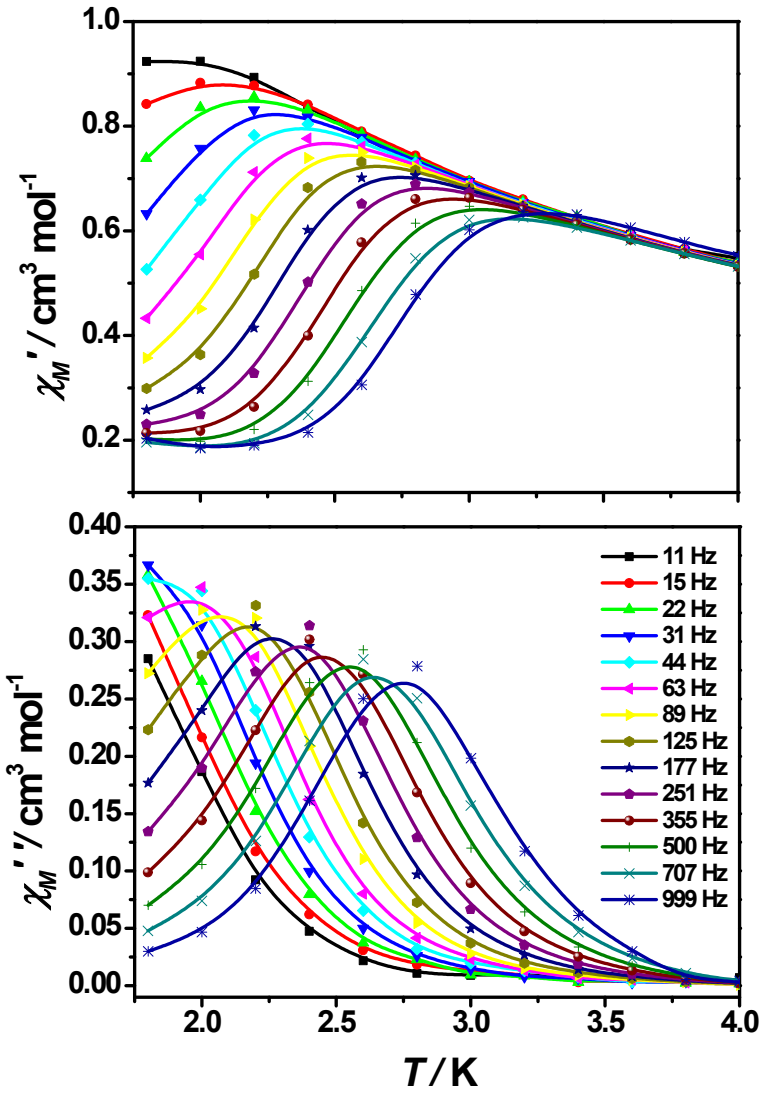

Fig. S29 Temperature dependence of in-of-phase (χ_M') and out-of-phase ac susceptibility (χ_M'') at different ac frequency under a 0.1 T dc field for **4**. The solid lines are for eye guide.

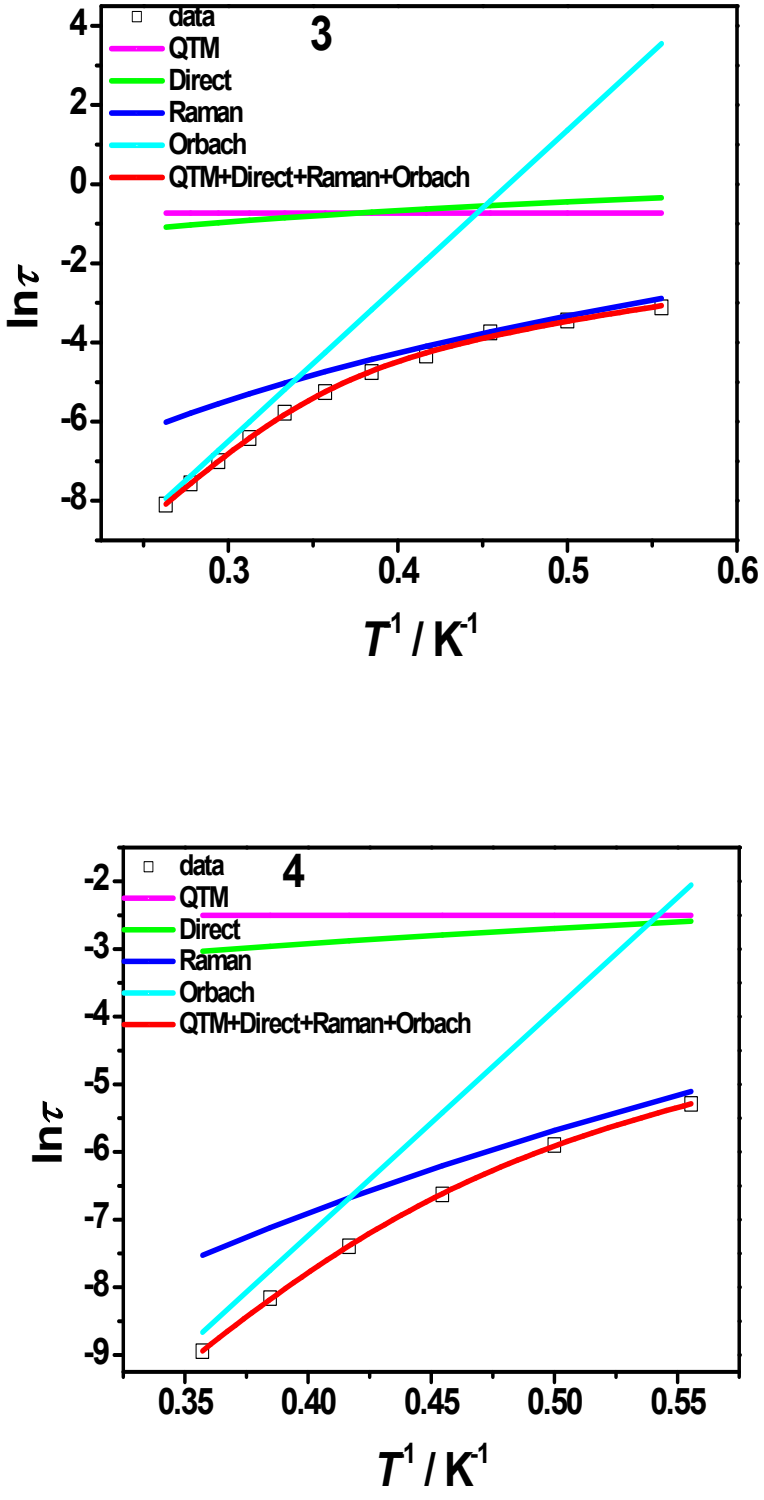

Fig. S30 Relaxation time of the magnetization *ln(τ)* vs T^{-1} plots for **3** and **4**.

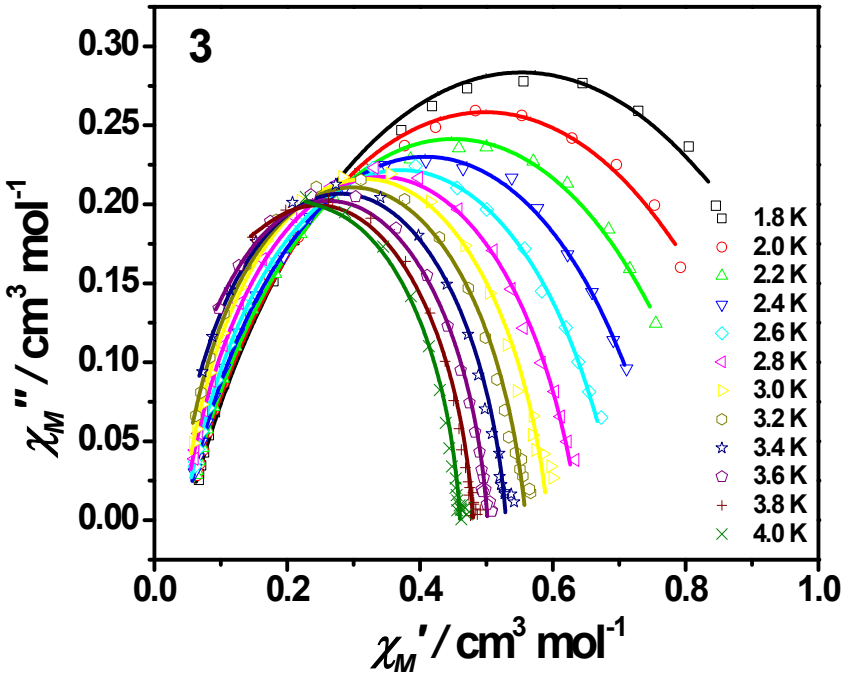

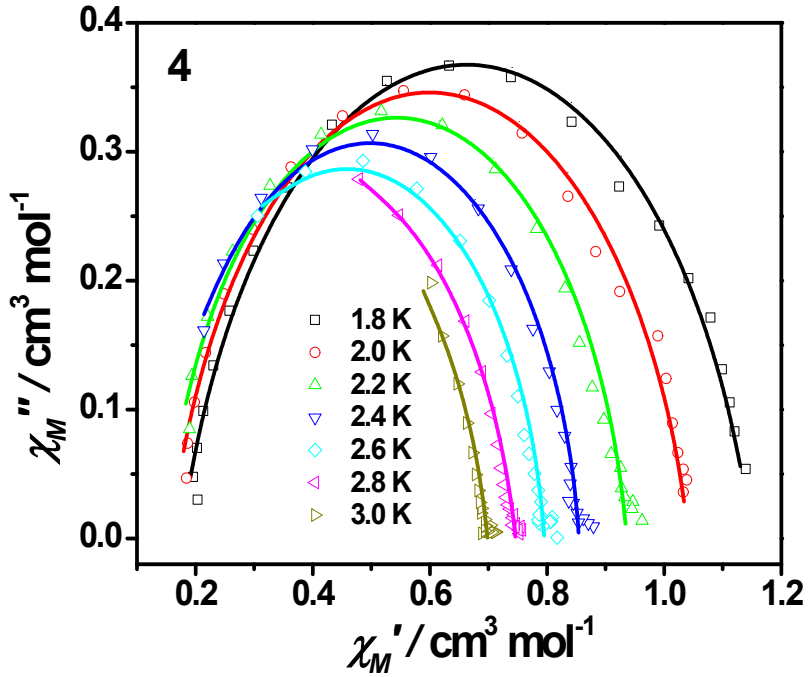

Fig. S31 Cole-Cole plot obtained from the ac susceptibility data under different range of temperature for **3** and **4**. Solid lines represent the best fits to a generalized Debye model[S6].

Table S8 Relaxation times τ (s) and α values for **1-4.**

1				
T (K)	χ_S	χ_T	τ (s)	α
1.8	0.14	2.07	0.37E-02	0.41
1.9	0.15	1.94	0.29E-02	0.38
2.0	0.16	1.82	0.24E-02	0.36
2.2	0.16	1.66	0.17E-02	0.34
2.6	0.17	1.43	0.10E-02	0.28
2.9	0.19	1.26	0.66E-03	0.23
3.3	0.20	1.13	0.44E-03	0.18
3.6	0.20	1.03	0.28E-03	0.14
4.0	0.20	0.94	0.17E-03	0.10
4.4	0.17E-05	0.86	0.57E-04	0.10
2				
T (K)	χ_S	χ_T	τ (s)	α
1.8	0.10	0.10	0.20E-02	0.33
1.9	0.10	0.94	0.18E-02	0.31
2.0	0.10	0.89	0.16E-02	0.29
2.2	0.10	0.82	0.13E-02	0.26
2.4	0.10	0.75	0.98E-03	0.22
2.6	0.10	0.70	0.76E-03	0.19
2.8	0.09	0.65	0.58E-03	0.16
3.0	0.09	0.61	0.44E-03	0.14
3.2	0.08	0.57	0.34E-03	0.13
3.4	0.07	0.54	0.25E-03	0.11
3.6	0.06	0.51	0.19E-03	0.09
3.8	0.03	0.49	0.13E-03	0.09
4.0	0.03	0.46	0.93E-04	0.08

3				
T (K)	χ_S	χ_T	τ (s)	α
1.8	0.05	1.06	0.36E-01	0.35
2.0	0.04	0.95	0.28E-01	0.34
2.2	0.04	0.86	0.20E-01	0.31
2.4	0.04	0.77	0.14E-01	0.28
2.6	0.04	0.70	0.90E-02	0.24
2.8	0.04	0.64	0.53E-02	0.19
3.0	0.04	0.59	0.30E-02	0.15
3.2	0.04	0.56	0.17E-02	0.13
3.4	0.03	0.53	0.93E-03	0.11
3.6	0.03	0.50	0.51E-03	0.09
3.8	0.01	0.48	0.29E-03	0.09
4.0	0.24E-11	0.46	0.16E-03	0.08
4				
T (K)	χ_S	χ_T	τ (s)	α
1.8	0.18	1.15	0.55E-02	0.17
2.0	0.16	1.04	0.30E-02	0.15
2.2	0.15	0.94	0.14E-02	0.11
2.4	0.14	0.85	0.63E-03	0.09
2.6	0.12	0.79	0.29E-03	0.09
2.8	0.01	0.75	0.11E-03	0.14
3.0	0.95E-15	0.70	0.49E-04	0.13

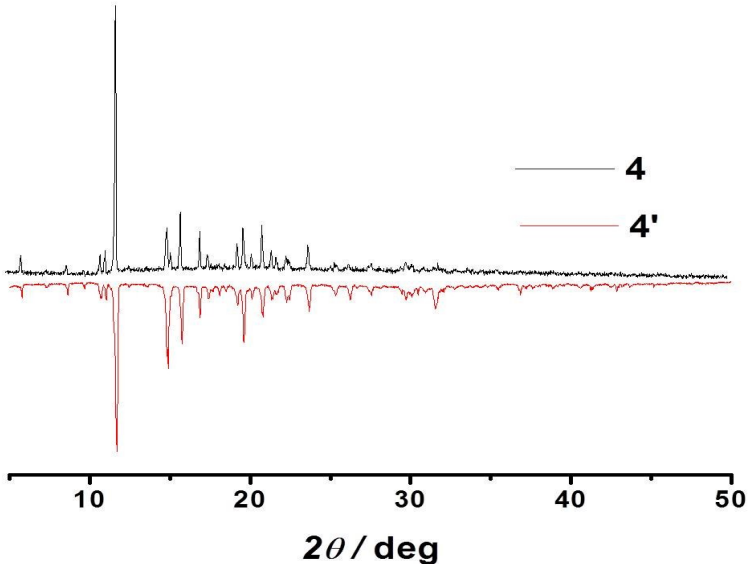

Fig. S32 XRD patterns for complex **4** and the diluted complex **4'**.

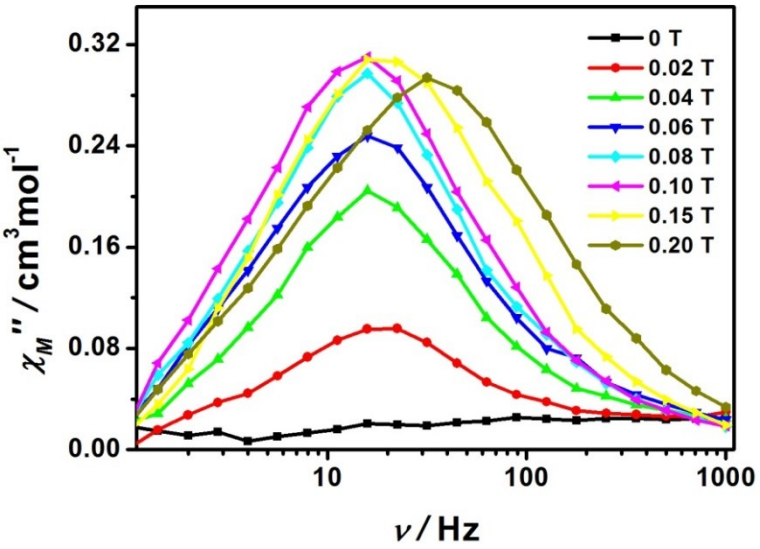

Fig. S33 Frequency dependence of out-of-phase (χ_M'') ac susceptibility at 1.8 K under the different applied static fields for **4'**. The solid lines are for eye guide.

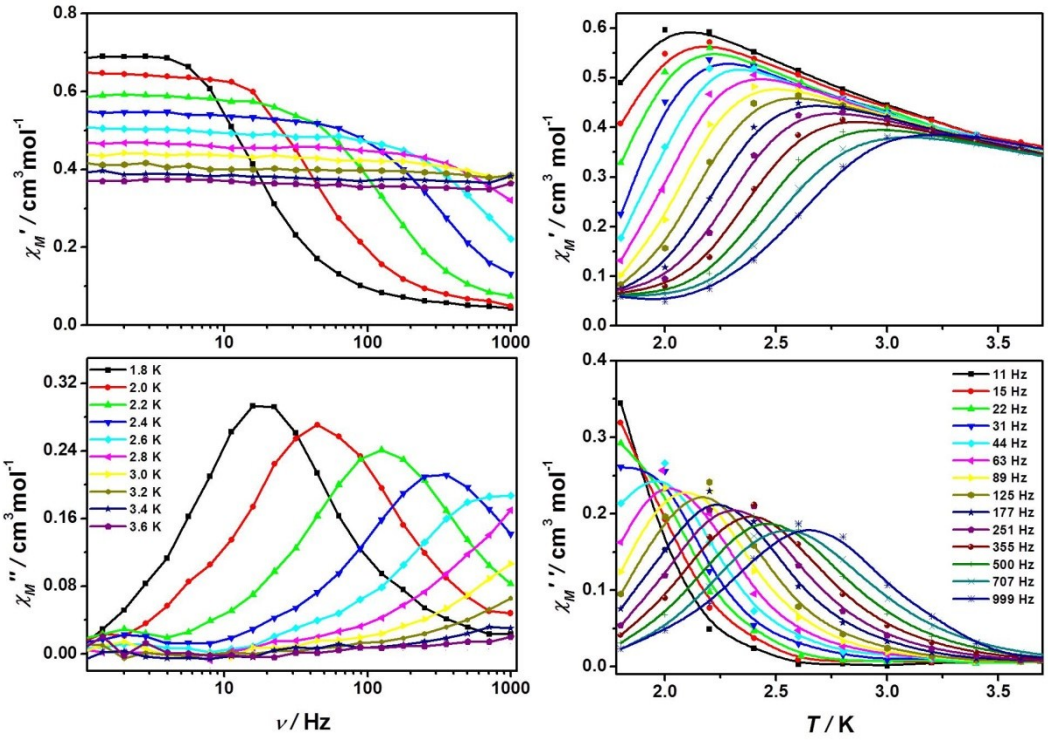

Fig. S34 Frequency and temperature dependence of the in-of-phase (χ_M') and out-of-phase (χ_M'') ac susceptibility under 0.10 T dc field for **4'**. The solid lines are for eye guide.

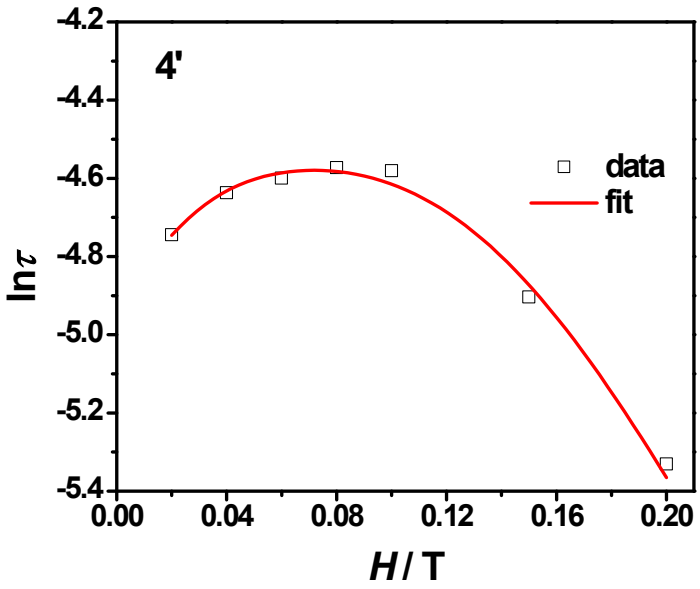

Fig. S35 Field dependence of the magnetization relaxation times for **4'**. The red line represents the best fit by using eqn (3).

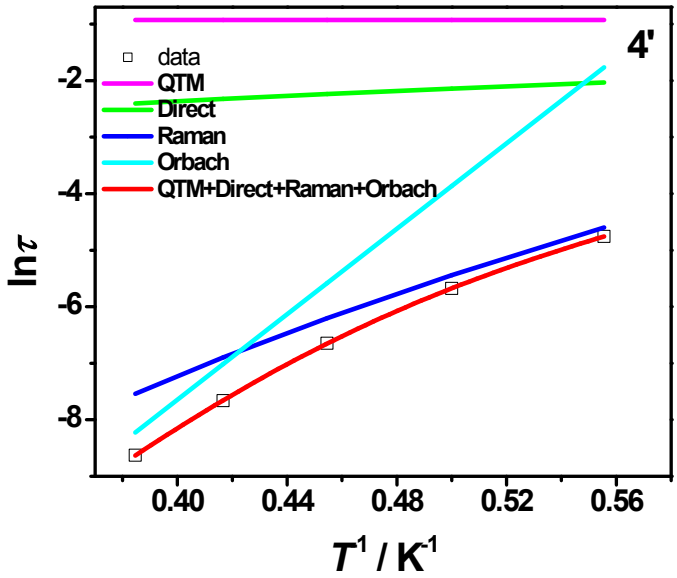

Fig. S36 Relaxation time of the magnetization *ln(τ)* vs T^{-1} plots for **4'**.

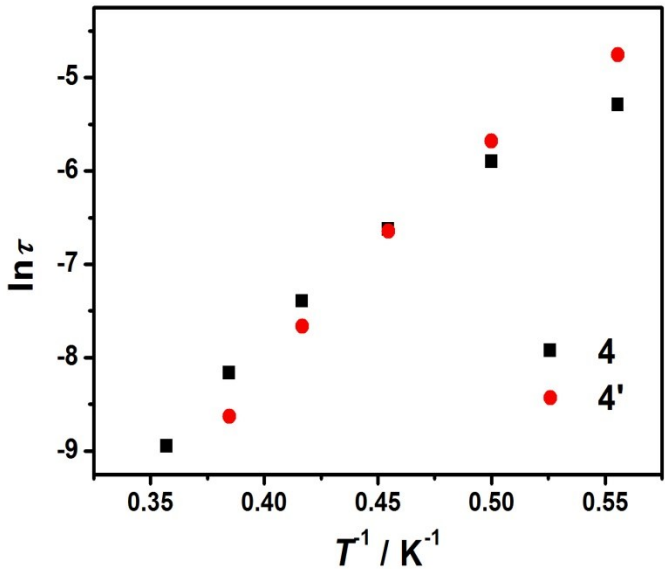

Fig. S37 Relaxation time of the magnetization ln(τ) vs T^{-1} plot for **4** and **4'** under the same dc field of 0.10 T.

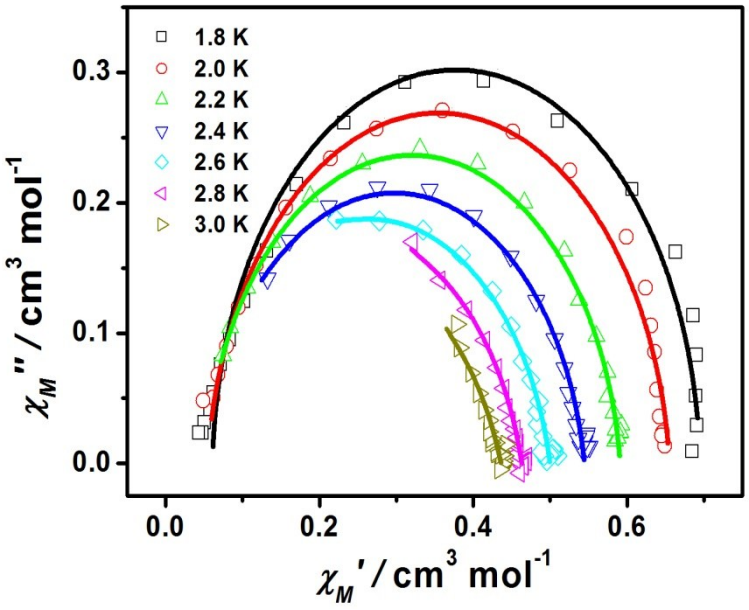

Fig. S38 Cole-Cole plot obtained from the ac susceptibility data under different temperature for **4'**. Solid lines represent the best fits to a generalized Debye model.

Table S9 Relaxation times τ (s) and α values for **4'.**

4'				
T (K)	χ_S	χ_T	τ (s)	α
1.8	0.06	0.69	0.83×10^{-2}	0.02
2.0	0.05	0.65	0.33×10^{-2}	0.06
2.2	0.05	0.59	0.12×10^{-2}	0.07
2.4	0.05	0.54	0.49×10^{-3}	0.10
2.6	0.03	0.50	0.20×10^{-3}	0.13
2.8	0.24×10^{-14}	0.46	0.88×10^{-4}	0.15
3.0	0.41×10^{-14}	0.44	0.39×10^{-4}	0.20

References

S1 (a) M. Llunell, D. Casanova, J. Cirera, P. Alemany and S. Alvarez, *Shape Program*, Version 2.1, 2013; (b) S. Alvarez, P. Alemany, D. Casanova, J. Cirera, M. Llunell and D. Avnir, *Coord. Chem. Rev.*, 2005, **249**, 1693-1708.

S2 N. F. Chilton, R. P. Anderson, L. D. Turner, A. Soncini and K. S. Murray, *J. Comput. Chem.*, 2013, **34**, 1164.

S3 Simulations were performed using SPIN developed by Andrew Ozarowski at the National High Magnetic Field Laboratory, USA.

S4 (a) F. Aquilante, L. De Vico, N. Ferré, G. Ghigo, P.-Å.Malmqvist, P. Neogrády, T. B. Pedersen, M. Pitonak, M. Reiher, B. O. Roos, L. Serrano-Andrés, M. Urban, V. Veryazov and R. Lindh, *J. Comput. Chem.*, 2010, **31**, 224; (b) V. Veryazov, P.-O. Widmark, L. Serrano-Andres, R. Lindh and B. O. Roos, *Int. J. Quantum Chem.*, 2004, **100**, 626; (c) G. Karlström, R. Lindh, P.-

Å. Malmqvist, B. O. Roos, U. Ryde, V. Veryazov, P.-O. Widmark, M. Cossi, B. Schimmelpfennig, P. Neograd y and L. Seijo, *Comput. Mater. Sci*., 2003, **28**, 222.

S5 (a) L. F. Chibotaru, L. Ungur and A. Soncini, *Angew. Chem. Int. Ed.*, 2008, **47**, 4126; (b) L. Ungur, W. Van den Heuvel and L. F. Chibotaru, *New J. Chem.*, 2009, **33**, 1224; (c) L. F. Chibotaru, L. Ungur, C. Aronica, H. Elmoll, G. Pilet and D. Luneau, *J. Am. Chem. Soc.*, 2008, **130**, 12445.

S6 (a) K. S. Cole and R. H. Cole, *J. Chem. Phys.*, 1941, **9**, 341; (b) Y.-N. Guo, G.-F. Xu, Y. Guo and J. Tang, *Dalton Trans.*, 2011, **40**, 9953-9963.